



Contents lists available at ScienceDirect

Ain Shams Engineering Journal

journal homepage: www.sciencedirect.com



Engineering Physics and Mathematics

G-L fractional differential operator modified using auto-correlation function: Texture enhancement in images

S. Hemalatha^{a,*}, S. Margret Anuncia^b^a School of Information Technology and Engineering, VIT University, Vellore 632014, Tamil Nadu, India^b School of Computer Science and Engineering, VIT University, Vellore 632014, Tamil Nadu, India

ARTICLE INFO

Article history:

Received 31 May 2016

Revised 18 October 2016

Accepted 12 December 2016

Available online xxx

Keywords:

Image texture

Fractional differentiation

Auto-correlation function

Texture enhancement

G-L definition

Gray level co-occurrence matrix

ABSTRACT

Texture plays an important role in the low-level image analysis and understanding in the field of computer vision. Texture based image enhancement is very important in many applications. In order to attain texture enhancement in images, a modified version of the Grunwald-Letnikov (G-L) definition based fractional differential operator is proposed in this paper. Considering the G-L based fractional differential operator's basic definition and implementation, a filter is devised and its applicability for texture enhancement is analyzed. Subsequently, the filter is modified by considering the auto-correlation effect between pixels in a neighborhood. Experiments are carried out on a number of standard texture-rich images and it is proved that the modified filter enhances the image contrast by nonlinearly enhancing the image textural features. In addition, the texture enhancement is quantitatively proven by a few Gray Level Co-occurrence Matrix (GLCM) measures, such as contrast, correlation, energy and homogeneity. Their % of Improvement is discussed in detail and the substantial improvement attained by the modified G-L FD operator over the basic G-L FD operator is well proved.

© 2016 Ain Shams University. Production and hosting by Elsevier B.V. This is an open access article under the CC BY-NC-ND license (<http://creativecommons.org/licenses/by-nc-nd/4.0/>).

1. Introduction

In most of the images, texture is considered to be the visual impression of coarseness or smoothness caused by the variability or uniformity of the image tone. Thus, the contribution of texture for low level image analysis is considered to be significant [1,2]. In general, image analysis that is accomplished by characterizing and representing image regions according to their texture content is called texture analysis. An image texture is analyzed to quantify instinctive properties, such as smoothness or coarseness. It is described to be a function of the spatial variation in pixel intensity levels.

Texture-based analysis of images is useful in a variety of applications and has been a subject of deep study by many researchers. In addition, the textural properties of an image are expected to expedite valuable information for analysis in domains such as remote sensing and medical imaging [3,4]. However, texture-based image analysis has many challenges to be addressed.

Primarily, the quality of the image needs to be improved to avoid the misinterpretation of images by the human visual system.

Usually, the quality of an image is improved through successive applications of image enhancement techniques [5–9], such as contrast stretching, histogram manipulation and unsharp masking. Histogram equalization-based image enhancement methods [8,9] are appropriate for images that have histograms with only single peak. Other enhancement methods [5–7] have restrictions for improving image textural features. In addition, these techniques provide major contributions for improving the statistical features such as mean and standard deviation of an image but only provide small improvements for textural features. Thus, a specific image enhancement technique is required as a pre-processing step that improves the textural features in images.

By visual interpretation, it is noticed that texture features are sharp details in images and it is inferred that differential operators may be considered for highlighting the textural information in images. Basically, first and second order differential operators such as gradient and Laplacian operators are used to highlight the edges and boundaries in images. It was also proved in the recent literature that fractional differential operators [10–12] are found to be more appropriate for image textural features than integral differential operators. Thus, fractional differential operators are considered for texture enhancement in images.

Peer review under responsibility of Ain Shams University.

* Corresponding author.

E-mail addresses: ishemalatha@gmail.com (S. Hemalatha), smargretanuncia@vit.ac.in (S. Margret Anuncia).<http://dx.doi.org/10.1016/j.asej.2016.12.003>

2090-4479/© 2016 Ain Shams University. Production and hosting by Elsevier B.V.

This is an open access article under the CC BY-NC-ND license (<http://creativecommons.org/licenses/by-nc-nd/4.0/>).

Please cite this article in press as: Hemalatha S, Margret Anuncia S. G-L fractional differential operator modified using auto-correlation function: Texture enhancement in images. Ain Shams Eng J (2017), <http://dx.doi.org/10.1016/j.asej.2016.12.003>

FD operators used in many image processing applications are devised in the form of filters to be operated on smaller neighborhoods in images; however, these filters do not include auto-correlation features that exist between pixels in a neighborhood. The detection of texture features using autocorrelation function is already proved in [13,14]. The existing texture analysis measures are thoroughly reviewed in [15], among which autocorrelation feature is formulated as one of the noteworthy texture measures. Hence, an attempt is made in this work to improve the G-L fractional differential filter by incorporating auto-correlation effect between neighbouring pixels.

The efficacy of the proposed FD operator needs to be proved using a texture characterization procedure. For texture characterization, various texture analysis approaches exist in the literature [1,2,16–19,3,4], where the spatial localities and rate of occurrences of intensity level differences pertaining to the image texture features are classified and categorized. Most researchers consider the process of texture analysis to be a process of texture segmentation [16,17], where the different regions of an image are treated as different texture classes, leading to a multi-texture segmentation problem. On comparing with approaches such as wavelet domain, Fourier domain, and statistical and structural methodologies of texture analysis, Gray-Level Co-occurrence Matrix (GLCM) method is found to be better for quantifying the image textural features [1]. Hence, the performance of the proposed texture enhancement filter is demonstrated using GLCM method. Therefore, modified G-L fractional differential operator is proposed for texture enhancement in images and the enhancement is quantified using the GLCM measures contrast, correlation, energy and homogeneity.

The remainder of the paper is organized as follows: The review of the related work is detailed in Section 2. The essential hypothetical background of the G-L definition of fractional differential is reviewed in Section 3 and the modified fractional differential filter is built in Section 4. Experimental results of the proposed method on test images are discussed in Section 5. The work is concluded in Section 6.

2. Related work

The aim of this section is to recollect the hypothetical background regarding the role of texture enhancement in image processing and its applications. Especially it concentrates on fractional differentiation and its progresses for texture enhancement. Some of the texture enhancement based applications are discussed in [20–25], where it is shown that texture enhancement plays a major role in the field of image processing and texture enhancement is an essential issue that needs to be considered in applications like remote sensing, medical imaging, image denoising, image interpretation, defect detection and image restoration.

In an application of segmenting fruit orchards from forests, an enhancing filter is applied to improve the spectral variation i.e. texture of these two bands prior to segmentation process [20]. Haar wavelet approximation coefficients are proposed to extract texture features in medical images in order to segment the prostate regions in a multi-resolution framework [21]. A texture enhancement methodology is suggested using Non local means (NL-means) algorithm for fabric defect detection [23]. In an image enhancement method based on histogram equalization, the textural features are employed in the contrast enhancement process in addition to the intensity information [25].

Since, FD operators are proposed for texture enhancement in this work, the evolution of fractional differentiation for textural features is discussed. The application of a fractional differential operator is initiated for edge identification using fractional calculus theory [26]. Attempts were made to map integer order derivatives

to fractional derivatives [10,11] that could be considered for texture enhancement in images. Cauchy integral derivatives are generalized to Riesz potential operators through fractional centred derivatives [10]. Riemann-Liouville's and Marchaud's derivatives are closely bound to fractional integrals over semi-infinite intervals [11] by the method of interpolation. Six fractional differential operators are devised based on two commonly used definitions of fractional differential, known as Grunwald-Letnikov(G-L) and Riemann-Liouville(R-L) for multiscale texture enhancement [12].

It has been proven by many researchers that the fractional differential operator is a robust operator for non-linearly enhancing image textural features and is useful in many applications [22,24,27–29]. Fractional differential based methodologies are proposed for enhancing textural details of remote sensing images [22] and for improving the registration of MR images [24]. The capability of one of the texture enhancing FD operators i.e. R-L FD operator for contrast enhancement is deliberated in [27]. A texture enhancement technique is introduced for medical images by using FD masks based on Srivastava-Owa fractional operators [28]. A set of fractional partial differential equation based multiscale denoising models are proposed for textured images [29].

In the recent literature, some improvements to the basic FD operators are made. Two adaptive FD operators based on G-L definition are proposed [30,31] to handle complex textures characterized by irregular patterns in images. In [30], G-L FD operator is refined with an adaptive fractional order to enhance regions that are both self-similar and non-regular in nature. In another approach [31], the adaptive fractional order is suggested to be obtained according to the dynamic gradient feature of the image. Variable Order Fractional Centred Difference (VOFCE) scheme [32] based on the second order Riesz FD operator is suggested to have dynamic adjustment for fractional order rather than having a constant value.

The improvements proposed for G-L FD operator in [30,31] are based on making the G-L FD order adaptive and changes made for second order Riesz FD operator [32] is about dynamically adjusting FD order; Whereas, The modification to the G-L FD operator made in this paper proposes to change the filter coefficients by considering the autocorrelation effect that exists between pixels in a neighbourhood. The autocorrelation feature is considered and included in the filter by distributing the weightage coefficient corresponding to one pixel in the basic G-L FD filter to all pixels having the same distance with the centre pixel in the modified filter. Thus, in case of choosing FD order in an adaptive manner or dynamically, the improvement is levied by fixing the fractional order to a particular value based on some of the properties specific to a pixel or an image region. The basic filter co-efficients do not change and remain the same. In the proposed solution, the improvement is imposed from within the operator by changing the filter co-efficients.

Especially, in the adaptive modifications that are suggested to the G-L fractional differential filter [30,31], the FD order is fixed to a particular value needing separate calculations that consider correlation between pixels and omit noise. For our proposed filter, the modifications are made by distributing the weightage coefficient of one pixel to many pixels and thereby considering correlation between pixels and omitting noise without the need for separate calculations.

3. Hypothetical analysis of fractional differential filter based on the G-L definition

According to the G-L definition of fractional differential, the differential operator is obtained in the integral differentiation definition by converting from integer to fraction [33,34]. Considering that $\forall v \in R$ (R -a set of real numbers, $[v]$ its integral part), the

one-dimensional signal $f(x) \in [a, x], a < x, a \in R, x \in R$, has an m ($m \in Z, Z$ a set of integers) - order analogous differentiation. Similarly, the ν -order differential is given by

$${}_a^C D_x^\nu f(x) = \lim_{h \rightarrow 0} {}_a^C D_h^\nu f(x) = \lim_{h \rightarrow 0} h^{-\nu} \sum_{m=0}^{n-1} \binom{-\nu}{m} f(x - mh) \quad (1)$$

where

$$\binom{-\nu}{m} = \frac{(-\nu)(-\nu+1)\dots(-\nu+m-1)}{m!} \quad (2)$$

From Eqs. (1) and (2), it is derived that

$$D_x^\nu = \sum_{m=0}^{n-1} \frac{\Gamma(m-\nu)}{\Gamma(m+1)} f(x - mh) \quad (3)$$

where h is the interval of one-dimensional signal being differentiated.

Next, the mathematical implementation of fractional differential filter for digital images is considered. The pixel values in digital images are finite and discrete and the distance between adjacent pixels is always one pixel. Therefore, the value of h must be 1 for fractional differential filter to be applied to images. The fractional differentiation of a 1- dimensional signal with $h = 1$ is represented as follows:

$$\begin{aligned} \frac{d^\nu f(x)}{dx^\nu} \approx & f(x) + (-\nu)f(x-1) + \frac{(-\nu)(-\nu+1)}{2}f(x-2) \\ & + \frac{(-\nu)(-\nu+1)(-\nu+2)}{6}f(x-3) + \dots \\ & + \frac{\Gamma(n-\nu)}{\Gamma(-\nu)\Gamma(n+1)}f(x-n) \end{aligned} \quad (4)$$

From Eq. (4), it is found that the first coefficient is a constant and that the remaining $n - 1$ coefficients are nonzero. The coefficients other than the first one are functions on the fractional order ν . It is also observed from mathematics that fractional differential has the following properties:

- i. At smooth pixel locations of images where the pixel values do not abruptly change or do not change at all, the fractional differential value varies from the highest at a particular point to zero slowly. In contrast to this, the corresponding value of integer differential is zero. Hence, the fractional differential value of a constant is not zero, which is not true for integer differential value.
- ii. At the origin stage of a slope of pixel values, the fractional differential value is not zero as is with integer differential.
- iii. Along the slope of gradual changes in the pixel values, the fractional differential is neither zero nor constant, whereas its integer differential is a constant.

Thus, it is evident that the sum of the coefficients in Eq. (4) is not zero, which is a noticeable difference between integral and fractional differentiation. In common, fractional differential can improve high-frequency texture features as well as maintain low-frequency contour information in images.

4. The modified design for G-L fractional differential filter

The modified G-L fractional differential operator is devised as a convolution filter as shown in this section. Essentially, a convolution filter is applied to all pixels in an image on a raster-scan fashion. It is obtained from the following expression

$$g(x, y) = \sum_{s=-a}^a \sum_{t=-b}^b w(s, t) f(x + s, y + t) \quad (5)$$

where $f(x, y)$ is a pixel value in the input image and $w(s, t)$ is a filter coefficient. The filter is derived to be an $N \times N$ matrix by taking into account the gradient direction. The filter has N layers and it has 8 different directions: $0, \frac{\pi}{8}, \frac{3\pi}{8}, \frac{\pi}{2}, \frac{5\pi}{8}, \frac{3\pi}{4}, \frac{7\pi}{8}$.

In order to have the numerical implementation in digital image processing, the 3×3 covering templates of the fractional differential operator are devised below. Considering Eq. (4), the partial fractional differential of $f(x, y)$ w.r.t. x is given as:

$$\frac{d^\nu f(x, y)}{dx^\nu} \approx f(x, y) + (-\nu)f(x-1, y) + \frac{(-\nu)(-\nu+1)}{2}f(x-2, y) \quad (6)$$

and the partial fractional differential of $f(x, y)$ w.r.t. y is given as:

$$\frac{d^\nu f(x, y)}{dy^\nu} \approx f(x, y) + (-\nu)f(x, y-1) + \frac{(-\nu)(-\nu+1)}{2}f(x, y-2) \quad (7)$$

The fractional differential covering templates on x and y coordinates are devised from Eqs. (6) and (7) and shown as follows:

Consequently, an attempt is made to modify the G-L fractional differential covering templates in order to improve the texture enhancement process. It is done by considering the fact that a huge amount of autocorrelation exists between pixels in a neighbourhood. Spatial autocorrelation signifies the dependency between values of a variable in neighboring locations [35]. It also represents a systematic pattern in values of a variable across the locations due to underlying common factors. This corresponds to texture features as they are repetitive patterns in images [14]. Hence, autocorrelation feature is found suitable to be used with FD operators to improve the process of texture enhancement. Usually, autocorrelation feature is measured by a function as the difference between an image $f(x, y)$ and the image shifted with a distance vector $f(x + dx, y + dy)$. As mentioned in [15], it can also be derived as a coefficient AC_{eff} and given in Eq. (8).

$$AC_{eff} = \frac{MN \sum_{x=1}^{M-dx} \sum_{y=1}^{N-dy} f(x, y) f(x + dx, y + dy)}{(M - dx)(N - dy) \sum_{x=1}^M \sum_{y=1}^N f^2(x, y)} \quad (8)$$

where $M \times N$ is the size of the input image considered and displacement in the x, y directions is denoted by dx and dy respectively. Since the texture primitives are periodic, the coefficient representing autocorrelation function increases or decreases periodically with dx and dy .

The improvisation of the G-L FD operator is attained based on the fact that the gray level of a pixel is not independent of its neighbours. The dependency of a pixel with its neighbor pixels is determined by the spatial autocorrelation function given in Eq. (8). The function has a value of 1, if only one pixel is considered, because a pixel is totally correlated with itself. It is also found to be true as and when $dx = dy = 0$ is substituted in Eq. (8). The value of the function decreases as the distance between two pixels increases, either horizontally or vertically. This behavior is incorporated into the G-L based fractional differential covering templates as follows:

In the G-L Fractional Differential filters shown above, the centre pixel of the 3×3 image region is assumed to be located in the third row, second column on x direction and it is located in the third column, second row on y direction. It is noticed in both of the 3×3 regions that there are 5 pixels on both x or y directions having one pixel displacement from the centre pixel and 3 pixels having two pixels displacement from the centre pixel. Out of 5 pixels having one pixel displacement from the center pixel, only 1 pixel is assigned with a coefficient of $-\nu$ and the remaining 4 pixels are assigned with a coefficient of 0 (see Table 1).

But, according to the autocorrelation function, all these 5 pixels are equally responsible for deciding the value of the centre pixel as they are located at the same distance from the centre pixel. Thus,

Table 1
G-L fractional differential filters.

0	$\frac{v^2-v}{2}$	0	0	0	0
0	$-v$	0	$\frac{v^2-v}{2}$	$-v$	1
0	1	0	0	0	0

Table 2
Demonstrating autocorrelation in G-L FD filters.

0	$\frac{v^2-v}{2}$	0	$\frac{v^2-v}{6}$	$\frac{v^2-v}{6}$	$\frac{v^2-v}{6}$
0	$-v$	0	$\frac{-v}{5}$	$\frac{-v}{5}$	$\frac{-v}{5}$
0	1	0	$\frac{-v}{5}$	1	$\frac{-v}{5}$

Table 3
Modified G-L fractional differential filters.

$\frac{v^2-v}{6}$	$\frac{v^2-v}{6}$	$\frac{v^2-v}{6}$	$\frac{v^2-v}{6}$	$\frac{-v}{5}$	$\frac{-v}{5}$
$\frac{-v}{5}$	$\frac{-v}{5}$	$\frac{-v}{5}$	$\frac{v^2-v}{2}$	$\frac{-v}{5}$	1
$\frac{-v}{5}$	1	$\frac{-v}{5}$	$\frac{v^2-v}{6}$	$\frac{-v}{5}$	$\frac{-v}{5}$

the weightage coefficient of these pixels must be made non-zero and equal. The weightage coefficient of v is equally shared among the 5 pixels by making their coefficients to be $-v/5$ in order to retain the proportion by weightage coefficient of $-v$ in Eqs. (6) and (7). This also facilitates to limit the intensity value of a pixel to be in the range $[0 - 255]$ after applying the proposed FD operator on images. Similarly, the coefficient of $(v^2 - v)/2$ assigned to one pixel in Fig. 6(a) and (b) is equally shared among the 3 pixels having an equal displacement with the center pixel and it is made to be $(v^2 - v)/6$. The modifications in the covering templates on x direction are demonstrated in Table 2.

The modified covering templates on x and y coordinates are presented in Table 3.

The result of adding all of the nonzero coefficients is not zero in the case of the fractional differential operator. Hence, constant or less varying pixel value in images has a non-zero response. Thus, the fractional differential operator non-linearly sustains texture details and facilitates texture enhancement. The mask discussed above is implemented on texture-rich images, and textural details are highlighted. To attain texture improvement, the input image is added to the fractional differential operated image pixel-by-pixel.

5. Experiments and analysis

The applicability and efficiency of the proposed fractional differential filter are verified by using test images from Brodatz database [36], Outex database [37] and the database of aerial images [38] and medical images [39]. The outex and Brodatz database contain thousands of grayscale and color texture images and there are 38 aerial images and many medical images in the database of aerial and medical images respectively. The proposed texture-enhancing filter is applied over more than 100 images from these databases and the results are encouraging. For demonstration, the results for 1 grayscale image from outex database, 1 grayscale and 2 color images from brodatz database are presented and analyzed. In addition, the texture-enhancing capability of the proposed G-L

FD operator is analyzed based on a texture characterization approach using GLCM method.

5.1. Selection of fractional order for the proposed method

Fractional differential filter basically imitates edge detection filter constructed with either $v = 1$ (first order derivatives) or $v = 2$ (second order derivatives). For FD operator, the value of v , the fractional order ranges from 0 to 2 in intervals of fractional values. It is already proven in [12] that the optimum value of v with the basic G-L FD operator is between 0 and 1. Thus, the convention is presumed to be continued for the modified FD operator. The modified G-L FD operator is implemented on various textured images and it is found that the degree of texture enhancement can be controlled by the order ranging from 0 to 1 in intervals of fractional values. Thus, when the modified G-L fractional differential filter is applied to texture enhancement in images, the optimum value of the parameter v should be chosen carefully.

The ultimate aim of the modified fractional differential operator is to enhance textural feature in images in an improved manner. The values for the fractional order should be chosen such that, the texture-enhancing filter must satisfy the following standards:

- i. It should highlight textural features.
- ii. It should preserve the high correlation between pixels while omitting the noise components.
- iii. It should increase the local contrast in the images.

It is well explained in Section 4, how the modified G-L FD operator is able to maintain the correlation between pixel values while enhancing the texture features as well as omitting the noise components.

With respect to finding the appropriate value for v , the proposed filter is applied to a set of images by varying the value of the fractional order v between 0 and 1, with an increment of 0.05. The results are analyzed to determine which value is satisfying the above standards. When such a trial is made by visual inspection on around 50 textured images, acceptable results are generated with v ranging from 0.5 to 0.7. In this paper, the fractional order chosen is demonstrated as the optimal value for two real time applications i.e. remote sensing and medical imaging. The analysis of how to find the optimum value for v by studying GLCM measures is given in Section 5.4.

5.2. Performance analysis using GLCM measures

In order to prove the effectiveness of the modified G-L fractional differential filter by quantitative measurement, Gray-Level Co-occurrence Matrix (GLCM) approach is used. The GLCM is an arrangement in matrix form that shows the different combinations of pixel values in an image. With GLCM, the relationship between two pixels is well exhibited by spatially relating them in different directions with regard to the distance between them. Thus, GLCM is described to be a 2-dimensional histogram of values for pixel pairs that are separated with a particular spatial relationship. Different GLCMs can be formed by changing distance between the pixels (preferably equal to 1) in a pair and at different rotation offsets such as $0^\circ, 45^\circ, 90^\circ, 135^\circ$ and so on. The computation of GLCM matrices is explained with an example given in Fig. 1. In Fig. 1(b), (i,j) signifies the frequency of occurrences of the pixel pair i,j with a particular distance and a specific rotation angle and is represented as $glc(i,j)$. The GLCM of the sample image with the distance of 1 and at two rotation angles 0° and 45° are shown in Fig. 1(d) and (e).

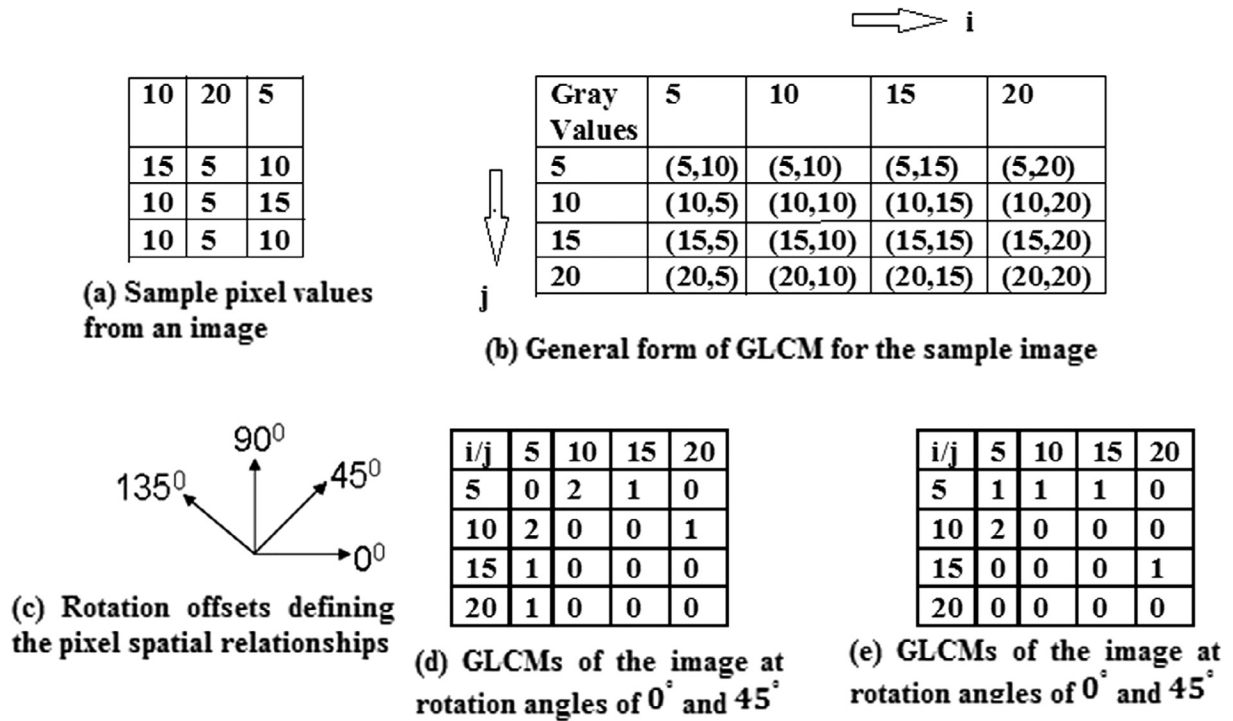


Fig. 1. Computing GLCM for a sample image.

Table 4
GLCM measures for texture analysis.

Measure	Description	Formula
Contrast	The local variations between the reference and neighbour pixels in the GLCM are measured Range: [0 to (size(GLCM) – 1)] ²	$\sum_{i,j} i - j ^2 glc(i,j)$
Correlation	The amount of linear-dependencies between values of reference and neighbour pixel over an image is measured Range: [-1 to +1]	$\sum_i \sum_j \frac{(i-\mu_i)(j-\mu_j)glc(i,j)}{\sigma_i \sigma_j}$
Energy	The number of repeated pairs and thus textural uniformity of the image is measured Range: [0 to 1]	$\sum_{i,j} glc(i,j)^2$
Homogeneity	The closeness of the reference pixel value and its neighbor is measured over the image Range: [0 to 1]	$-\sum_{i,j} glc(i,j) \log_2 glc(i,j)$

Table 5
Parameters used in GLCM measures.

Parameter	Description	Range of Values
<i>i</i>	Reference pixel value	Minimum and maximum pixel values in an image
<i>j</i>	Neighbour pixel value	Minimum and maximum pixel values in an image
<i>glc(i,j)</i>	An entry in GLCM	0 and the maximum number of occurrences of the pixel pair <i>i</i> and <i>j</i>
μ_i, μ_j	Means of GLCM w.r.t. <i>i</i> and <i>j</i>	Depending on GLCM entries
σ_i, σ_j	Standard deviations of GLCM w.r.t. <i>i</i> and <i>j</i>	Depending on GLCM entries

In GLCM approach, texture is defined by the statistical relationship between two pixels, namely the reference and neighbor pixels. Consequently, all of the pixels in the image take the role of a

reference pixel in turn. The texture measures contrast, correlation, energy and homogeneity that are derived from the GLCM are statistic in nature and most frequently used in the literature [1]. Therefore, these measures are used for justifying the texture enhancement performance of the proposed FD operator. The four measures are listed in Table 4 with their description and formula.

The parameters used for calculating the above measures are listed in Table 5 with their description and range of values.

Thus, for the quantitative evaluation with GLCM approach, an offset matrix is created at 4 different rotation offsets i.e. 0°, 45°, 90°, 135°. The GLCM is generated from the original image, G-L FD operated images and modified G-L FD operated images. Then, from the generated GLCM, four statistical texture measures contrast, correlation, energy and homogeneity are calculated. This process is repeated for different values of fractional order ranging from $\nu = 0$ to $\nu = 1$.

5.3. Evaluation by visual analysis

Figs. 2–5 show the results obtained from histogram equalization [8,9], basic G-L fractional differential operator [11] and the modified G-L fractional differential operator. By observing the results, it is noted that the Histogram Equalization method concentrates on enhancing the image contrast excessively, but the texture enhancement is less likely to be concentrated. The basic G-L FD operator enhances the image textural features. However, this method does not take into consideration the high degree of autocorrelation that exists between pixels, and thus usually ignore local texture features. Thus, in spite of providing productivity in overall texture enhancement, this method is not able to concentrate on enhancing local texture patterns and preserve minute features like small edges. The modified G-L fractional differential operator results in better enhancement of textural features, enhancing local texture patterns and also preserves small edges in images leading to provide more encouraging results.

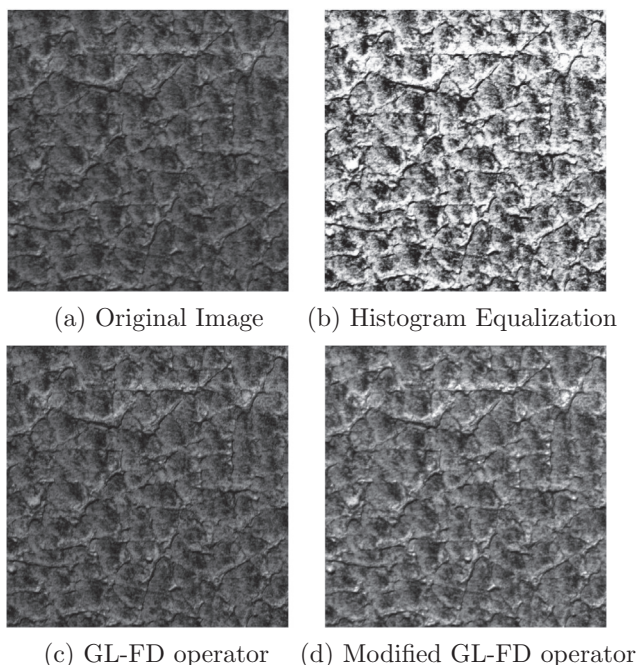


Fig. 2. Sample Image 1 - Brodatz album (grayscale).

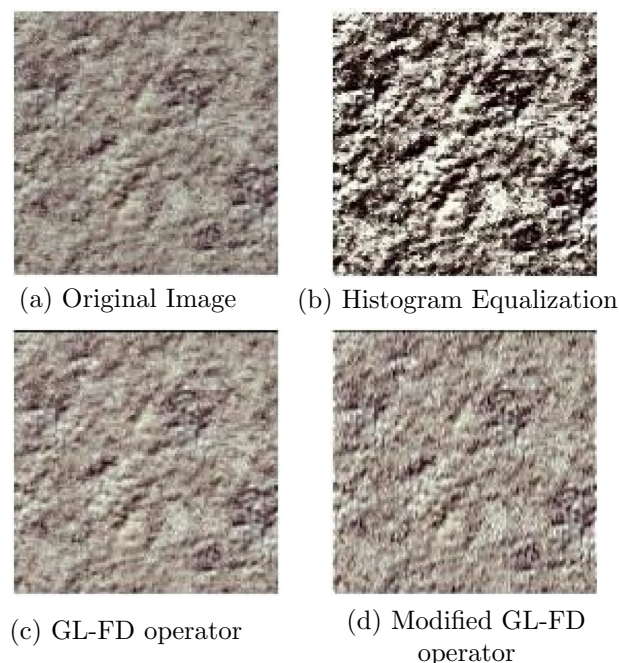


Fig. 4. Sample Image 3 - Brodatz album (color).

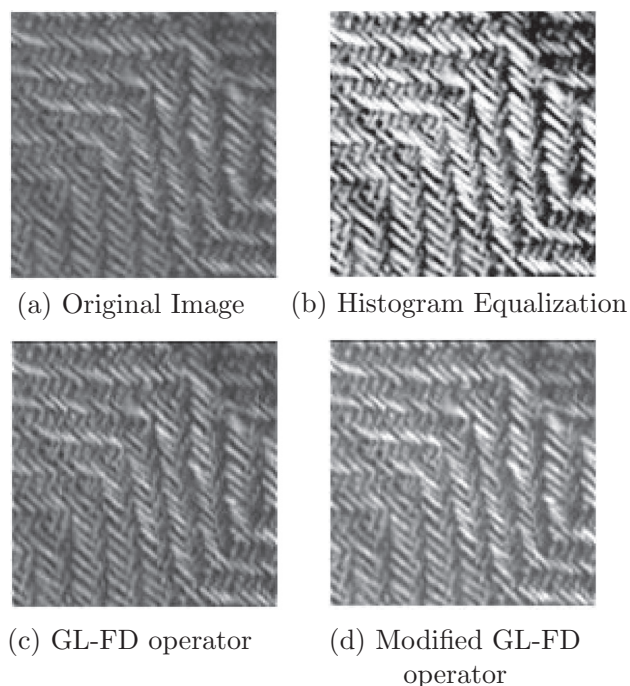


Fig. 3. Sample Image 2 - Outex album (grayscale).

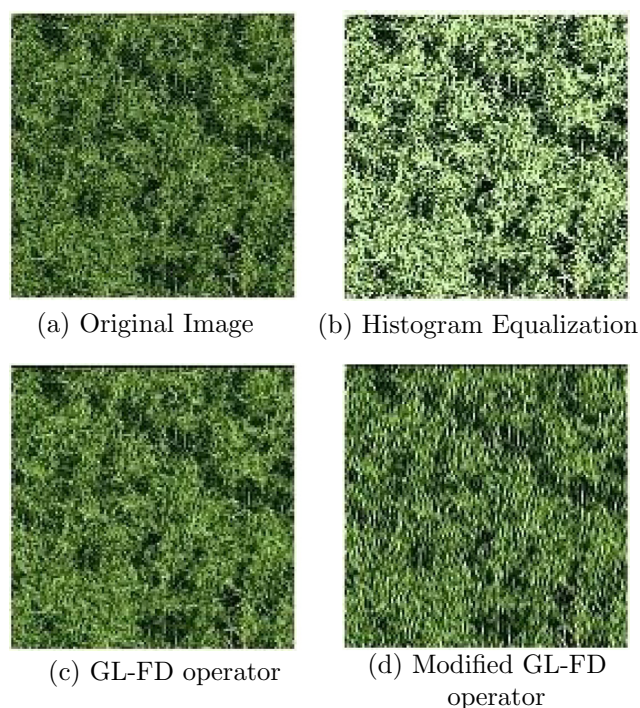


Fig. 5. Sample Image 4 - Brodatz album (color).

5.4. Evaluation by GLCM measures

The GLCM measures contrast, correlation, energy and homogeneity are computed for the four images presented in Figs. 2–5 in order to justify the improvisation attained by the modified G-L FD operator over the basic G-L FD operator.

5.4.1. Contrast

Contrast is measured as sum of variance squares multiplied by the spatial frequency, reflecting the variation between the

reference and neighbor pixel over an entire image. It is understood that the similar pixel values result in low contrast and hence produces a weak dissemination of texture features. Applying FD operators helps to increase contrast in images and thereby increasing texture strength.

The contrast measure is evaluated as per the formula given in Table 4 with the Percentage of Contrast Improvement ($\%C_{imp}$) defined as follows:

$$\%C_{imp} = (C_{FD} - C_I) / C_I * 100 \quad (9)$$

where C_{FD} is the contrast of the FD operated image and C_i is the contrast of the input image.

As an increase in contrast signifies the increased texture strength, positive values of $\%C_{imp}$ indicate the improvement. The contrast measure calculated for the four images (Figs. 2–5) with the $\%C_{imp}$ obtained by the basic G-L FD operator (G-L FD op.) and by the modified G-L FD operator (M G-L FD op.) is presented in Tables 6–9.

Referring Tables 6–9, it is observed that the modified G-L FD operator provides a more significant increase in $\%C_{imp}$ over the basic G-L FD operator and thereby is able to increase the depth of textural information in images better than the basic G-L FD operator. It is also noted that the basic G-L FD operator is able to increase the contrast when ν is increased from 0 to 0.5 beyond

which the contrast decreases resulting in loss of textural information. With the modified G-L FD operator, the contrast increases considerably when ν is increased from 0 to 1. Thus, the range of values of ν , for which texture enhancement is attained, is also increased by the proposed FD operator.

5.4.2. Correlation

Correlation is a measure of how correlated a reference pixel to its neighbor over an image. Higher values of correlation imply a linear relationship between the gray levels of pixel pairs. Hence, a drop in this measure indicates better clarity of texture details. Correlation is highly uncorrelated to contrast, as the likelihood values of two pixels is completely independent from contrast.

Table 6
Sample Image 1 - contrast.

Fractional order	0°				45°				90°				135°			
	G-L op.	$\%C_{imp}$	M G-L op.	$\%C_{imp}$	G-L op.	$\%C_{imp}$	M G-L op.	$\%C_{imp}$	G-L op.	$\%C_{imp}$	M G-L op.	$\%C_{imp}$	G-L op.	$\%C_{imp}$	M G-L op.	$\%C_{imp}$
Input Image	0.5906	0.00	0.5906	0.00	0.8170	0.00	0.8170	0.00	0.7619	0.00	0.7619	0.00	1.0914	0.00	1.0914	0.00
Output Image (v=0)	0.3655	-38.12	0.3655	-38.12	0.5221	-36.09	0.5221	-36.09	0.4406	-42.18	0.4406	-42.18	0.7183	-34.18	0.7183	-34.18
Output Image (v=0.05)	0.4257	-27.92	0.4411	-25.32	0.6000	-26.55	0.6091	-25.45	0.5113	-32.89	0.5121	-32.79	0.8460	-22.49	0.8562	-21.55
Output Image (v=0.15)	0.5453	-7.68	0.6007	1.71	0.7819	-4.30	0.8118	-0.63	0.6548	-14.06	0.6513	-14.52	1.0936	0.20	1.1367	4.15
Output Image (v=0.25)	0.6557	11.02	0.7660	29.69	0.9612	17.65	1.0195	24.79	0.8165	7.16	0.8031	5.40	1.3507	23.76	1.4235	30.43
Output Image (v=0.35)	0.7483	26.70	0.9574	62.10	1.1019	34.87	1.2410	51.90	0.9621	26.27	0.9480	24.42	1.5720	44.04	1.7325	58.74
Output Image (v=0.45)	0.8088	36.93	1.1010	86.42	1.2095	48.05	1.3716	67.88	1.0511	37.95	1.0111	32.71	1.6958	55.38	1.9101	75.02
Output Image (v=0.55)	0.8096	37.07	1.1864	100.88	1.2290	50.44	1.4516	77.68	1.0748	41.06	1.0320	35.44	1.6975	55.54	1.9794	81.37
Output Image (v=0.65)	0.7627	29.13	1.2423	110.33	1.1705	43.27	1.4622	78.97	1.0448	37.12	0.9999	31.23	1.6062	47.17	1.9818	81.58
Output Image (v=0.75)	0.7148	21.02	1.2594	113.24	1.1362	39.07	1.4352	75.67	1.0303	35.23	0.9271	21.68	1.5216	39.42	1.8946	73.60
Output Image (v=0.85)	0.6612	11.95	1.2415	110.20	1.0342	26.59	1.3658	67.18	0.9459	24.14	0.8568	12.45	1.3793	26.38	1.8093	65.78
Output Image (v=0.95)	0.6133	3.83	1.2511	111.82	0.9807	20.03	1.3320	63.04	0.9121	19.71	0.7993	4.90	1.2779	17.09	1.7213	57.72
Output Image (v=1)	0.5889	-0.29	1.2635	113.94	0.9421	15.31	1.3212	61.71	0.8871	16.43	0.7675	0.73	1.2158	11.40	1.6917	55.01

Table 7
Sample Image 2 - contrast.

Fractional order	0°				45°				90°				135°			
	G-L op.	$\%C_{imp}$	M G-L op.	$\%C_{imp}$	G-L op.	$\%C_{imp}$	M G-L op.	$\%C_{imp}$	G-L op.	$\%C_{imp}$	M G-L op.	$\%C_{imp}$	G-L op.	$\%C_{imp}$	M G-L op.	$\%C_{imp}$
Input Image	2.7081	0.00	2.7081	0.00	2.9462	0.00	2.9462	0.00	2.5324	0.00	2.5324	0.00	2.8474	0.00	2.8474	0.00
Output Image (v=0)	4.5502	68.02	4.5502	68.02	4.8603	64.97	4.8603	64.97	2.3311	-7.95	2.3311	-7.95	4.7939	68.36	4.7939	68.36
Output Image (v=0.05)	4.6004	69.87	4.8225	78.08	4.9091	66.62	5.1225	73.87	2.3906	-5.60	2.4274	-4.14	4.8351	69.81	5.0411	77.05
Output Image (v=0.15)	4.5482	67.95	5.3034	95.83	4.8830	65.74	5.5428	88.13	2.4285	-4.10	2.5363	0.16	4.7748	67.69	5.4657	91.96
Output Image (v=0.25)	4.3799	61.73	5.6313	107.94	4.6965	59.41	5.7983	96.81	2.4347	-3.86	2.5945	2.45	4.5757	60.70	5.6994	100.17
Output Image (v=0.35)	4.1449	53.06	5.9208	118.63	4.4616	51.44	5.9802	102.98	2.4264	-4.19	2.6250	3.66	4.3625	53.21	5.8715	106.21
Output Image (v=0.45)	3.8589	42.49	6.1150	125.80	4.1362	40.39	6.0647	105.85	2.3803	-6.01	2.6043	2.84	4.0520	42.31	5.9752	109.85
Output Image (v=0.55)	3.5409	30.75	6.2383	130.36	3.7942	28.78	6.0831	106.48	2.2975	-9.27	2.5678	1.40	3.7004	29.96	6.0037	110.85
Output Image (v=0.65)	3.2726	20.85	6.3065	132.88	3.5437	20.28	6.0424	105.09	2.2938	-9.42	2.5252	-0.28	3.4530	21.27	5.9528	109.06
Output Image (v=0.75)	3.0766	13.61	6.3041	132.78	3.3360	13.23	5.9695	102.62	2.3209	-8.35	2.4176	-4.53	3.2491	14.11	5.8601	105.81
Output Image (v=0.85)	2.8750	6.16	6.3091	132.97	3.1337	6.37	5.8497	98.55	2.3801	-6.01	2.3387	-7.65	3.0528	7.22	5.7932	103.46
Output Image (v=0.95)	2.7227	0.54	6.3205	133.39	3.0026	1.92	5.7710	95.88	2.4681	-2.54	2.2883	-9.64	2.9108	2.23	5.7155	100.73
Output Image (v=1)	2.7054	-0.10	6.2934	132.39	2.9852	1.32	5.7049	93.64	2.5735	1.62	2.2565	-10.89	2.8900	1.50	5.6617	98.84

Table 8
Sample Image 3 - contrast.

Fractional order	0°				45°				90°				135°			
	G-L op.	$\%C_{imp}$	M G-L op.	$\%C_{imp}$	G-L op.	$\%C_{imp}$	M G-L op.	$\%C_{imp}$	G-L op.	$\%C_{imp}$	M G-L op.	$\%C_{imp}$	G-L op.	$\%C_{imp}$	M G-L op.	$\%C_{imp}$
Input Image	0.5271	0.00	0.5271	0.00	0.7706	0.00	0.7706	0.00	0.5823	0.00	0.5823	0.00	0.6198	0.00	0.6198	0.00
Output Image (v=0)	0.4919	-6.66	0.4919	-6.66	0.7181	-6.81	0.7181	-6.81	0.4255	-26.92	0.4255	-26.92	0.5949	-4.02	0.5949	-4.02
Output Image (v=0.05)	0.5265	-0.10	0.5433	3.09	0.7736	0.40	0.7886	2.34	0.4613	-20.77	0.4649	-20.16	0.6372	2.81	0.6519	5.19
Output Image (v=0.15)	0.5849	10.97	0.6435	22.10	0.8644	12.17	0.9184	19.18	0.5246	-9.91	0.5364	-7.87	0.7126	14.99	0.7639	23.25
Output Image (v=0.25)	0.6334	20.18	0.7432	41.01	0.9429	22.36	1.0424	35.27	0.5777	-0.78	0.5969	2.51	0.7718	24.53	0.8638	39.37
Output Image (v=0.35)	0.6603	25.27	0.8271	56.94	0.9914	28.65	1.1381	47.69	0.6166	5.89	0.6409	10.07	0.8066	30.14	0.9458	52.60
Output Image (v=0.45)	0.6675	26.65	0.8964	70.08	1.0135	31.52	1.2095	56.95	0.6390	9.74	0.6691	14.90	0.8185	32.07	1.0078	62.61
Output Image (v=0.55)	0.6626	25.71	0.9469	79.66	1.0112	31.22	1.2526	62.55	0.6534	12.21	0.6818	17.09	0.8130	31.18	1.0427	68.24
Output Image (v=0.65)	0.6383	21.11	0.9781	85.58	0.9805	27.24	1.2629	63.89	0.6504	11.70	0.6759	16.07	0.7875	27.07	1.0557	70.34
Output Image (v=0.75)	0.6053	14.85	0.9929	88.39	0.9367	21.56	1.2470	61.82	0.6397	9.87	0.6565	12.74	0.7486	20.78	1.0522	69.77
Output Image (v=0.85)	0.5744	8.98	1.0037	90.44	0.8843	14.76	1.2230	58.71	0.6264	7.57	0.6344	8.95	0.7049	13.74	1.0359	67.14
Output Image (v=0.95)	0.5418	2.79	1.0055	90.78	0.8152	5.78	1.1820	53.38	0.6061	4.10	0.6037	3.67	0.6572	6.05	1.0122	63.32
Output Image (v=1)	0.5286	0.29	1.0018	90.07	0.7922	2.80	1.1552	49.92	0.6026	3.48	0.5861	0.65	0.6401	3.28	0.9966	60.81

Table 9
Sample Image 4 - contrast.

Rotation offset Fractional order	0°				45°				90°				135°			
	G-L op.	%Cor _{Imp}	M G-L op.	%Cor _{Imp}	G-L op.	%Cor _{Imp}	M G-L op.	%Cor _{Imp}	G-L op.	%Cor _{Imp}	M G-L op.	%Cor _{Imp}	G-L op.	%Cor _{Imp}	M G-L op.	%Cor _{Imp}
Input Image	0.5145	0.00	0.5145	0.00	0.6675	0.00	0.6675	0.00	0.4818	0.00	0.4818	0.00	0.6418	0.00	0.6418	0.00
Output Image (v=0)	0.2946	-42.73	0.2946	-42.73	0.3961	-40.66	0.3961	-40.66	0.2342	-51.38	0.2342	-51.38	0.3852	-39.99	0.3852	-39.99
Output Image (v=0.05)	0.3413	-33.66	0.3549	-31.02	0.4600	-31.09	0.4718	-29.32	0.2707	-43.81	0.2729	-43.36	0.4459	-30.52	0.4582	-28.61
Output Image (v=0.15)	0.4506	-12.41	0.5040	-2.04	0.6067	-9.12	0.6537	-2.07	0.3539	-26.53	0.3611	-25.06	0.5831	-9.15	0.6283	-2.11
Output Image (v=0.25)	0.5709	10.97	0.6861	33.36	0.7676	14.99	0.8698	30.31	0.4443	-7.78	0.4583	-4.86	0.7341	14.38	0.8317	29.58
Output Image (v=0.35)	0.6917	34.46	0.8994	74.84	0.9276	38.96	1.1087	66.09	0.5428	12.67	0.5606	16.35	0.8867	38.16	1.0591	65.02
Output Image (v=0.45)	0.7540	46.56	1.0676	107.53	1.0058	50.67	1.2828	92.16	0.6039	25.35	0.6267	30.09	0.9648	50.32	1.2270	91.18
Output Image (v=0.55)	0.6978	35.64	1.1085	115.47	0.9421	41.13	1.3053	95.54	0.5820	20.80	0.6218	29.06	0.9010	40.38	1.2492	94.64
Output Image (v=0.65)	0.6629	28.85	1.1334	120.32	0.8936	33.86	1.3018	95.02	0.5716	18.65	0.6031	25.19	0.8586	33.78	1.2455	94.06
Output Image (v=0.75)	0.5946	15.57	1.1266	118.98	0.8097	21.29	1.2656	89.59	0.5363	11.32	0.5715	18.63	0.7748	20.72	1.2074	88.13
Output Image (v=0.85)	0.5519	7.27	1.1222	118.13	0.7508	12.48	1.2297	84.21	0.5137	6.63	0.5406	12.22	0.7190	12.03	1.1782	83.58
Output Image (v=0.95)	0.5374	4.45	1.1500	123.55	0.7253	8.65	1.2309	84.40	0.5198	7.89	0.5271	9.42	0.6982	8.79	1.1787	83.65
Output Image (v=1)	0.5166	0.41	1.1585	125.20	0.6960	4.26	1.2252	83.55	0.5090	5.66	0.5175	7.43	0.6703	4.44	1.1734	82.83

Correlation is measured by the formula given in Table 4. The Percentage of correlation Improvement (%Cor_{Imp}) is defined as follows:

$$\%Cor_{Imp} = (Cor_{FD} - Cor_i) / Cor_i * 100 \tag{10}$$

where Cor_{FD} is the correlation of the FD operated image and Cor_i is the correlation of the input image.

With diminishing values of correlation, texture details are more clearly visible and thus, negative values of %Cor_{Imp} indicate texture

enhancement. The correlation is evaluated for four texture images in Figs. 2–5 alongwith the %Cor_{Imp} and are shown in Tables 10–13.

It is noticed from Tables 10–13 that the correlation decreases with increasing fractional differential order indicating better clarity of texture details. Also, the %Cor_{Imp} provided by the modified G-L FD operator is more than that provided by the basic G-L FD operator. When v reaches closer to 1, %Cor_{Imp} achieved with G-L FD operator is almost ignorable when compared with that achieved by the modified operator. Hence, the process of improving texture enhancement is proved.

Table 10
Sample Image 1 - correlation.

Rotation offset Fractional order	0°				45°				90°				135°			
	G-L op.	%Cor _{Imp}	M G-L op.	%Cor _{Imp}	G-L op.	%Cor _{Imp}	M G-L op.	%Cor _{Imp}	G-L op.	%Cor _{Imp}	M G-L op.	%Cor _{Imp}	G-L op.	%Cor _{Imp}	M G-L op.	% Imp.
Input Image	0.6947	0.00	0.6947	0.00	0.5789	0.00	0.5789	0.00	0.6077	0.00	0.6077	0.00	0.4375	0.00	0.4375	0.00
Output Image (v=0)	0.7026	1.14	0.7026	1.14	0.5551	-4.11	0.5551	-4.11	0.6255	2.92	0.6255	2.92	0.3866	-11.63	0.3866	-11.63
Output Image (v=0.05)	0.7102	2.23	0.7007	0.86	0.5717	-1.25	0.5679	-1.90	0.6357	4.61	0.6373	4.87	0.3947	-9.77	0.3914	-10.54
Output Image (v=0.15)	0.7250	4.35	0.7009	0.89	0.5889	1.72	0.5810	0.36	0.6566	8.03	0.6642	9.29	0.4239	-3.12	0.4124	-5.73
Output Image (v=0.25)	0.7430	6.95	0.7029	1.17	0.6079	5.01	0.5921	2.28	0.6676	9.85	0.6788	11.70	0.4482	2.45	0.4298	-1.75
Output Image (v=0.35)	0.7519	8.23	0.6932	-0.22	0.6208	7.23	0.5922	2.29	0.6694	10.15	0.6885	13.29	0.4582	4.72	0.4302	-1.67
Output Image (v=0.45)	0.7548	8.64	0.6755	-2.78	0.6201	7.11	0.5867	1.35	0.6704	10.31	0.6955	14.44	0.4667	6.67	0.4240	-3.07
Output Image (v=0.55)	0.7522	8.27	0.6540	-5.87	0.6095	5.28	0.5679	-1.91	0.6590	8.44	0.6936	14.12	0.4599	5.13	0.4105	-6.18
Output Image (v=0.65)	0.7499	7.94	0.6232	-10.30	0.6000	3.64	0.5480	-5.34	0.6434	5.87	0.6923	13.92	0.4503	2.92	0.3871	-11.52
Output Image (v=0.75)	0.7490	7.81	0.5893	-15.18	0.5816	0.47	0.5233	-9.61	0.6213	2.24	0.6945	14.28	0.4389	0.33	0.3703	-15.35
Output Image (v=0.85)	0.7389	6.35	0.5583	-19.64	0.5715	-1.29	0.5059	-12.62	0.6086	0.14	0.6935	14.11	0.4278	-2.22	0.3450	-21.13
Output Image (v=0.95)	0.7302	5.11	0.5191	-25.28	0.5479	-5.36	0.4793	-17.21	0.5799	-4.58	0.6923	13.91	0.4102	-6.23	0.3267	-25.32
Output Image (v=1)	0.7278	4.76	0.4953	-28.71	0.5437	-6.08	0.4636	-19.92	0.5709	-6.06	0.6937	14.15	0.4106	-6.14	0.3127	-28.52

Table 11
Sample Image 2 - correlation.

Rotation offset Fractional order	0°				45°				90°				135°			
	G-L op.	%Cor _{Imp}	M G-L op.	%Cor _{Imp}	G-L op.	%Cor _{Imp}	M G-L op.	%Cor _{Imp}	G-L op.	%Cor _{Imp}	M G-L op.	%Cor _{Imp}	G-L op.	%Cor _{Imp}	M G-L op.	% Imp.
Input Image	0.2215	0.00	0.2215	0.00	0.1544	0.00	0.1544	0.00	0.2724	0.00	0.2724	0.00	0.1827	0.00	0.1827	0.00
Output Image (v=0)	0.3332	50.44	0.3332	50.44	0.2855	84.98	0.2855	84.98	0.6568	141.11	0.6568	141.11	0.2953	61.59	0.2953	61.59
Output Image (v=0.05)	0.3240	46.30	0.3069	38.55	0.2764	79.04	0.2617	69.54	0.6471	137.55	0.6496	138.49	0.2873	57.20	0.2734	49.63
Output Image (v=0.15)	0.3178	43.48	0.2559	15.53	0.2646	71.43	0.2200	42.53	0.6337	132.63	0.6425	135.88	0.2809	53.73	0.2308	26.33
Output Image (v=0.25)	0.3038	37.16	0.2023	-8.66	0.2501	62.06	0.1766	14.42	0.6106	124.18	0.6311	131.69	0.2694	47.44	0.1907	4.34
Output Image (v=0.35)	0.2930	32.28	0.1459	-34.12	0.2350	52.24	0.1356	-12.18	0.5832	114.11	0.6201	127.66	0.2520	37.90	0.1513	-17.22
Output Image (v=0.45)	0.2808	0.00	0.0888	0.00	0.2247	0.00	0.0948	0.00	0.5533	0.00	0.6111	0.00	0.2405	0.00	0.1082	0.00
Output Image (v=0.55)	0.2722	22.92	0.0388	-82.48	0.2150	39.29	0.0614	-60.23	0.5240	92.36	0.6038	121.68	0.2344	28.29	0.0737	-59.68
Output Image (v=0.65)	0.2700	21.92	-	-105.38	0.2035	31.82	0.0291	-81.12	0.4838	77.62	0.5945	118.25	0.2239	22.51	0.0435	-76.17
Output Image (v=0.75)	0.2572	16.13	-	-125.63	0.1876	21.55	-	-101.14	0.4342	59.41	0.5948	118.36	0.2088	14.27	0.0166	-90.91
Output Image (v=0.85)	0.2510	13.32	-	-145.93	0.1769	14.64	-	-114.39	0.3743	37.41	0.5921	117.38	0.1982	8.47	-	-106.75
Output Image (v=0.95)	0.2448	10.53	-	-165.66	0.1611	4.37	-	-129.91	0.3099	13.76	0.5863	115.25	0.1868	2.21	-	-119.75
Output Image (v=1)	0.2362	6.67	-	-174.23	0.1516	-1.81	-	-136.13	0.2679	-1.66	0.5836	114.27	0.1786	-2.26	-	-126.12

Table 12
Sample Image 3 - correlation.

Rotation offset Fractional order	0°				45°				90°				135°			
	G-L op.	%Cor _{Imp}	M G-L op.	%Cor _{Imp}	G-L op.	%Cor _{Imp}	M G-L op.	%Cor _{Imp}	G-L op.	%Cor _{Imp}	M G-L op.	%Cor _{Imp}	G-L op.	%Cor _{Imp}	M G-L op.	% Imp.
Input Image	0.8466	0.00	0.8466	0.00	0.7759	0.00	0.7759	0.00	0.8307	0.00	0.8307	0.00	0.8197	0.00	0.8197	0.00
Output Image (v=0)	0.8766	3.54	0.8766	3.54	0.8191	5.57	0.8191	5.57	0.8930	7.50	0.8930	7.50	0.8501	3.71	0.8501	3.71
Output Image (v=0.05)	0.8759	3.45	0.8722	3.02	0.8169	5.28	0.8138	4.89	0.8909	7.26	0.8904	7.19	0.8491	3.59	0.8460	3.21
Output Image (v=0.15)	0.8753	3.38	0.8637	2.02	0.8149	5.04	0.8049	3.74	0.8878	6.88	0.8861	6.68	0.8474	3.38	0.8377	2.19
Output Image (v=0.25)	0.8734	3.16	0.8534	0.80	0.8108	4.51	0.7938	2.31	0.8842	6.45	0.8820	6.18	0.8451	3.10	0.8291	1.14
Output Image (v=0.35)	0.8721	3.01	0.8426	-0.47	0.8073	4.05	0.7829	0.91	0.8802	5.97	0.8778	5.68	0.8432	2.86	0.8196	-0.02
Output Image (v=0.45)	0.8707	2.85	0.8313	-1.82	0.8030	3.50	0.7718	-0.53	0.8759	5.45	0.8738	5.20	0.8409	2.58	0.8098	-1.21
Output Image (v=0.55)	0.8690	2.65	0.8195	-3.21	0.7993	3.02	0.7606	-1.96	0.8704	4.78	0.8698	4.71	0.8386	2.31	0.8007	-2.32
Output Image (v=0.65)	0.8683	2.56	0.8073	-4.65	0.7968	2.70	0.7506	-3.25	0.8653	4.16	0.8667	4.34	0.8368	2.08	0.7915	-3.44
Output Image (v=0.75)	0.8672	2.43	0.7936	-6.26	0.7935	2.28	0.7403	-4.58	0.8590	3.42	0.8635	3.95	0.8350	1.86	0.7809	-4.74
Output Image (v=0.85)	0.8624	1.86	0.7760	-8.34	0.7872	1.47	0.7266	-6.34	0.8493	2.25	0.8584	3.34	0.8304	1.30	0.7684	-6.26
Output Image (v=0.95)	0.8512	0.54	0.7478	-11.67	0.7751	-1.10	0.7031	-9.38	0.8328	0.26	0.8487	2.17	0.8187	-0.13	0.7457	-9.03
Output Image (v=1)	0.8486	0.23	0.7375	-12.89	0.7721	-0.48	0.6968	-10.20	0.8267	-0.48	0.8465	1.91	0.8158	-0.47	0.7384	-9.92

Table 13
Sample Image 4 - correlation.

Rotation offset Fractional order	0°				45°				90°				135°			
	G-L op.	%Cor _{Imp}	M G-L op.	%Cor _{Imp}	G-L op.	%Cor _{Imp}	M G-L op.	%Cor _{Imp}	G-L op.	%Cor _{Imp}	M G-L op.	%Cor _{Imp}	G-L op.	%Cor _{Imp}	M G-L op.	% Imp.
Input Image	0.7205	0.00	0.7205	0.00	0.6371	0.00	0.6371	0.00	0.7385	0.00	0.7385	0.00	0.6511	0.00	0.6511	0.00
Output Image (v=0)	0.8149	13.11	0.8149	13.11	0.7480	17.40	0.7480	17.40	0.8514	15.29	0.8514	15.29	0.7548	15.93	0.7548	15.93
Output Image (v=0.05)	0.8161	13.28	0.8099	12.42	0.7491	17.59	0.7444	16.83	0.8528	15.48	0.8525	15.44	0.7567	16.22	0.7516	15.45
Output Image (v=0.15)	0.8167	13.37	0.7978	10.73	0.7507	17.83	0.7353	15.42	0.8549	15.76	0.8540	15.65	0.7603	16.77	0.7455	14.51
Output Image (v=0.25)	0.8097	12.38	0.7761	7.72	0.7416	16.39	0.7139	12.05	0.8507	15.20	0.8494	15.02	0.7527	15.61	0.7264	11.57
Output Image (v=0.35)	0.7964	10.54	0.7439	3.25	0.7243	13.69	0.6822	7.07	0.8390	13.60	0.8395	13.67	0.7364	13.10	0.6963	6.95
Output Image (v=0.45)	0.7817	8.50	0.7087	-1.63	0.7061	10.83	0.6478	1.67	0.8238	11.56	0.8281	12.13	0.7180	10.28	0.6630	1.84
Output Image (v=0.55)	0.7794	8.18	0.6792	-5.72	0.6988	9.68	0.6199	-2.71	0.8142	10.26	0.8192	10.93	0.7119	9.33	0.6362	-2.29
Output Image (v=0.65)	0.7678	6.57	0.6421	-10.88	0.6833	7.24	0.5864	-7.96	0.7977	8.02	0.8088	9.52	0.6956	6.83	0.6043	-7.19
Output Image (v=0.75)	0.7588	5.32	0.6043	-16.13	0.6668	4.66	0.5529	-13.22	0.7797	5.58	0.7987	8.16	0.6811	4.60	0.5734	-11.93
Output Image (v=0.85)	0.7522	4.41	0.5695	-20.95	0.6583	3.33	0.5258	-17.48	0.7666	3.81	0.7924	7.30	0.6727	3.32	0.5456	-16.21
Output Image (v=0.95)	0.7352	2.04	0.5292	-26.55	0.6379	0.12	0.4936	-22.53	0.7409	0.32	0.7843	6.20	0.6513	0.04	0.5150	-20.90
Output Image (v=1)	0.7288	1.16	0.5098	-29.24	0.6298	-1.15	0.4790	-24.81	0.7296	-1.20	0.7812	5.78	0.6433	-1.19	0.5010	-23.05

5.4.3. Energy

The GLCM measure energy reflects textural uniformity. Thus, a decrease in energy implies more irregularity and inhomogeneity in the change of texture and texture enhancement is justified.

Energy is measured with the formula in Table 4. The Percentage of Energy Improvement (%E_{Imp}) is defined as follows:

$$\%E_{Imp} = (E_{FD} - E_I) / E_I * 100 \tag{11}$$

where E_{FD} is the energy of the FD operated image and E_I is the energy of the input image.

Since, texture enhancement is justified by a decrease in energy, negative values of %E_{Imp} signify texture enhancement. The energy

measure computed together with %E_{Imp} for the images in Figs. 2–5 are presented in Tables 14–17.

Tables 14–17 justify the enhancement attained by the modified FD operator in terms of energy and %E_{Imp}, since the energy decreases more swiftly with the modified G-L FD operator than with the basic G-L FD operator.

5.4.4. Homogeneity

The closeness of gray levels in spatial distribution is measured over the image as homogeneity. Higher the values of homogeneity, more close are the pixel values that identify uniform image regions. Therefore, a fall with this measure reveals texture enhancement.

Table 14
Sample Image 1 - energy.

Rotation offset Fractional order	0°				45°				90°				135°			
	G-L op.	%E _{Imp}	M G-L op.	%E _{Imp}	G-L op.	%E _{Imp}	M G-L op.	%E _{Imp}	G-L op.	%E _{Imp}	M G-L op.	%E _{Imp}	G-L op.	%E _{Imp}	M G-L op.	%E _{Imp}
Input Image	0.1263	0.00	0.1263	0.00	0.1112	0.00	0.1117	0.00	0.1134	0.00	0.1134	0.00	0.1002	0.00	0.1002	0.00
Output Image (v=0)	0.6122	384.91	0.6122	384.91	0.6019	441.46	0.6019	438.89	0.6088	436.82	0.6088	436.82	0.5698	468.92	0.5698	468.92
Output Image (v=0.05)	0.5550	339.60	0.5536	338.46	0.5437	389.10	0.5431	386.23	0.5542	388.64	0.5541	388.59	0.5107	409.98	0.5099	409.18
Output Image (v=0.15)	0.4181	231.16	0.4092	224.11	0.4042	263.57	0.3969	255.30	0.4184	268.92	0.4152	266.13	0.3717	271.16	0.3647	264.16
Output Image (v=0.25)	0.2734	116.54	0.2630	108.28	0.2577	131.77	0.2509	124.57	0.2679	136.26	0.2679	136.22	0.2304	130.03	0.2251	124.75
Output Image (v=0.35)	0.1587	25.68	0.1508	19.45	0.1455	30.84	0.1414	26.61	0.1529	34.81	0.1567	38.20	0.1268	26.57	0.1242	24.01
Output Image (v=0.45)	0.0977	-22.59	0.0873	-30.88	0.0869	-21.80	0.0820	-26.59	0.0935	-17.54	0.0935	-17.52	0.0761	-24.01	0.0720	-28.09
Output Image (v=0.55)	0.0847	-32.93	0.0696	-44.90	0.0747	-32.80	0.0655	-41.35	0.0795	-29.93	0.0761	-32.93	0.0657	-34.39	0.0586	-41.52
Output Image (v=0.65)	0.0901	-28.66	0.0684	-45.85	0.0797	-28.33	0.0654	-41.41	0.0843	-25.71	0.0762	-32.85	0.0707	-29.39	0.0591	-40.96
Output Image (v=0.75)	0.0975	-22.76	0.0721	-42.89	0.0868	-21.95	0.0696	-37.72	0.0902	-20.43	0.0816	-28.01	0.0761	-24.00	0.0635	-36.56
Output Image (v=0.85)	0.1066	-15.56	0.0762	-39.68	0.0941	-15.32	0.0744	-33.42	0.0989	-12.78	0.0883	-22.18	0.0844	-15.78	0.0679	-32.17
Output Image (v=0.95)	0.1165	-7.73	0.0797	-36.86	0.1021	-8.19	0.0794	-28.96	0.1055	-7.01	0.0950	-16.24	0.0923	-7.87	0.0729	-27.19
Output Image (v=1)	0.1234	-2.26	0.0819	-35.10	0.1089	-2.06	0.0820	-26.60	0.1111	-2.04	0.0988	-12.89	0.0980	-2.15	0.0757	-24.46

Table 15
Sample Image 2 - energy.

Rotation offset Fractional order	0°				45°				90°				135°			
	G-L op.	%E _{Imp}	M G-L op.	%E _{Imp}	G-L op.	%E _{Imp}	M G-L op.	%E _{Imp}	G-L op.	%E _{Imp}	M G-L op.	%E _{Imp}	G-L op.	%E _{Imp}	M G-L op.	%E _{Imp}
Input Image	0.0440	0.00	0.0440	0.00	0.0432	0.00	0.0432	0.00	0.0448	0.00	0.0448	0.00	0.0433	0.00	0.0433	0.00
Output Image (v=0)	0.0285	-35.29	0.0285	-35.29	0.0279	-35.52	0.0279	-35.52	0.0394	-12.07	0.0394	-12.07	0.0281	-35.01	0.0281	-35.01
Output Image (v=0.05)	0.0261	-40.78	0.0257	-41.73	0.0256	-40.85	0.0252	-41.70	0.0346	-22.66	0.0347	-22.44	0.0257	-40.60	0.0254	-41.45
Output Image (v=0.15)	0.0242	-45.05	0.0225	-48.89	0.0237	-45.24	0.0222	-48.58	0.0302	-32.54	0.0295	-34.08	0.0239	-44.92	0.0223	-48.45
Output Image (v=0.25)	0.0249	-43.39	0.0217	-50.66	0.0245	-43.42	0.0215	-50.17	0.0299	-33.23	0.0276	-38.32	0.0246	-43.23	0.0216	-50.12
Output Image (v=0.35)	0.0267	-39.31	0.0217	-50.79	0.0262	-39.34	0.0216	-50.13	0.0313	-30.06	0.0272	-39.20	0.0263	-39.24	0.0216	-50.18
Output Image (v=0.45)	0.0293	-33.45	0.0224	-49.25	0.0287	-33.49	0.0222	-48.58	0.0337	-24.69	0.0280	-37.50	0.0289	-33.33	0.0223	-48.48
Output Image (v=0.55)	0.0323	-26.77	0.0232	-47.34	0.0317	-26.64	0.0232	-46.42	0.0365	-18.41	0.0291	-35.06	0.0318	-26.49	0.0232	-46.47
Output Image (v=0.65)	0.0350	-20.57	0.0244	-44.66	0.0345	-20.25	0.0244	-43.65	0.0388	-13.41	0.0307	-31.51	0.0345	-20.25	0.0243	-43.86
Output Image (v=0.75)	0.0378	-14.19	0.0258	-41.44	0.0372	-14.00	0.0258	-40.41	0.0408	-8.92	0.0329	-26.59	0.0373	-13.97	0.0257	-40.58
Output Image (v=0.85)	0.0405	-8.06	0.0274	-37.83	0.0399	-7.73	0.0274	-36.64	0.0426	-4.78	0.0353	-21.09	0.0399	-7.88	0.0273	-36.88
Output Image (v=0.95)	0.0429	-2.70	0.0291	-33.99	0.0420	-2.73	0.0291	-32.75	0.0440	-1.70	0.0378	-15.53	0.0420	-2.96	0.0290	-33.09
Output Image (v=1)	0.0436	-1.02	0.0300	-31.93	0.0427	-1.23	0.0299	-30.80	0.0442	-1.27	0.0390	-12.85	0.0428	-1.25	0.0298	-31.13

Table 16
Sample Image 3 - energy.

Rotation offset Fractional order	0°				45°				90°				135°			
	G-L op.	%E _{Imp}	M G-L op.	%E _{Imp}	G-L op.	%E _{Imp}	M G-L op.	%E _{Imp}	G-L op.	%E _{Imp}	M G-L op.	%E _{Imp}	G-L op.	%E _{Imp}	M G-L op.	%E _{Imp}
Input Image	0.0981	0.00	0.0981	0.00	0.0852	0.00	0.0852	0.00	0.0945	0.00	0.0945	0.00	0.0919	0.00	0.0919	0.00
Output Image (v=0)	0.2095	113.55	0.2095	113.55	0.1940	127.64	0.1940	127.64	0.2168	129.41	0.2168	129.41	0.2014	119.22	0.2014	119.22
Output Image (v=0.05)	0.1772	80.60	0.1760	79.41	0.1622	90.35	0.1613	89.31	0.1835	94.21	0.1832	93.86	0.1695	84.50	0.1686	83.50
Output Image (v=0.15)	0.1282	30.72	0.1251	27.55	0.1147	34.60	0.1125	32.02	0.1326	40.39	0.1318	39.52	0.1216	32.39	0.1191	29.69
Output Image (v=0.25)	0.0965	-1.60	0.0921	-6.09	0.0846	-0.75	0.0818	-4.03	0.1000	5.84	0.0991	4.90	0.0908	-1.21	0.0877	-4.56
Output Image (v=0.35)	0.0794	-19.10	0.0733	-25.28	0.0683	-19.87	0.0645	-24.26	0.0816	-13.66	0.0803	-15.05	0.0741	-19.32	0.0697	-24.18
Output Image (v=0.45)	0.0728	-25.79	0.0642	-34.55	0.0617	-27.54	0.0565	-33.70	0.0742	-21.52	0.0715	-24.32	0.0674	-26.66	0.0612	-33.38
Output Image (v=0.55)	0.0712	-27.41	0.0605	-38.32	0.0606	-28.93	0.0538	-36.92	0.0720	-23.79	0.0686	-27.44	0.0661	-28.01	0.0582	-36.64
Output Image (v=0.65)	0.0746	-23.91	0.0608	-38.06	0.0635	-25.44	0.0546	-35.96	0.0747	-20.91	0.0698	-26.08	0.0692	-24.69	0.0589	-35.91
Output Image (v=0.75)	0.0807	-17.73	0.0633	-35.44	0.0689	-19.09	0.0576	-32.39	0.0801	-15.27	0.0742	-21.51	0.0747	-18.66	0.0619	-32.64
Output Image (v=0.85)	0.0872	-11.07	0.0663	-32.41	0.0750	-11.96	0.0612	-28.22	0.0855	-9.50	0.0788	-16.61	0.0811	-11.70	0.0653	-28.88
Output Image (v=0.95)	0.0944	-3.81	0.0696	-29.05	0.0817	-4.08	0.0651	-23.60	0.0915	-3.13	0.0842	-10.84	0.0883	-3.90	0.0694	-24.46
Output Image (v=1)	0.0972	-0.95	0.0714	-27.27	0.0843	-1.03	0.0672	-21.12	0.0935	-0.99	0.0869	-8.01	0.0909	-1.01	0.0715	-22.19

Table 17
Sample Image 4 - energy.

Rotation offset Fractional order	0°				45°				90°				135°			
	G-L op.	%E _{Imp}	M G-L op.	%E _{Imp}	G-L op.	%E _{Imp}	M G-L op.	%E _{Imp}	G-L op.	%E _{Imp}	M G-L op.	%E _{Imp}	G-L op.	%E _{Imp}	M G-L op.	%E _{Imp}
Input Image	0.1383	0.00	0.1383	0.00	0.1246	0.00	0.1246	0.00	0.1407	0.00	0.1407	0.00	0.1261	0.00	0.1261	0.00
Output Image (v=0)	0.5346	286.58	0.5346	286.58	0.5204	317.52	0.5204	317.52	0.5490	290.24	0.5490	290.24	0.5234	315.21	0.5234	315.21
Output Image (v=0.05)	0.4829	249.21	0.4800	247.11	0.4678	275.35	0.4652	273.29	0.4983	254.20	0.4969	253.20	0.4711	273.70	0.4684	271.53
Output Image (v=0.15)	0.3705	167.91	0.3619	161.72	0.3546	184.51	0.3473	178.66	0.3880	175.82	0.3841	173.00	0.3582	184.13	0.3507	178.22
Output Image (v=0.25)	0.2506	81.19	0.2397	73.32	0.2355	88.97	0.2268	81.99	0.2683	90.70	0.2654	88.63	0.2382	88.92	0.2297	82.20
Output Image (v=0.35)	0.1416	2.41	0.1315	-4.94	0.1297	4.04	0.1228	-1.47	0.1562	11.03	0.1558	10.75	0.1314	4.27	0.1246	-1.20
Output Image (v=0.45)	0.0895	-35.26	0.0768	-44.45	0.0807	-35.28	0.0718	-42.42	0.0990	-29.61	0.0952	-32.34	0.0818	-35.14	0.0728	-42.22
Output Image (v=0.55)	0.1028	-25.67	0.0785	-43.27	0.0926	-25.67	0.0736	-40.95	0.1111	-21.02	0.0960	-31.75	0.0938	-25.57	0.0745	-40.91
Output Image (v=0.65)	0.0989	-28.51	0.0760	-45.06	0.0889	-28.64	0.0721	-42.12	0.1062	-24.50	0.0954	-32.20	0.0901	-28.53	0.0730	-42.07
Output Image (v=0.75)	0.1253	-9.40	0.0856	-38.08	0.1131	-9.26	0.0816	-34.51	0.1315	-6.51	0.1070	-23.98	0.1144	-9.24	0.0826	-34.44
Output Image (v=0.85)	0.1289	-6.76	0.0904	-34.66	0.1160	-6.92	0.0868	-30.38	0.1344	-4.45	0.1147	-18.44	0.1175	-6.77	0.0879	-30.31
Output Image (v=0.95)	0.1242	-10.16	0.0862	-37.70	0.1117	-10.40	0.0838	-32.79	0.1277	-9.21	0.1123	-20.16	0.1131	-10.31	0.0847	-32.79
Output Image (v=1)	0.1366	-1.24	0.0884	-36.10	0.1230	-1.28	0.0861	-30.90	0.1389	-1.25	0.1152	-18.13	0.1244	-1.32	0.0872	-30.87

Homogeneity is measured with the formula in Table 4. The Percentage of Homogeneity Improvement (%H_{Imp}) is defined as follows:

$$\%H_{Imp} = (H_{FD} - H_I) / E_I * 100 \tag{12}$$

where H_{FD} is the homogeneity of the FD operated image and H_I is the homogeneity of the input image. Negative values of %H_{Imp} defend improved textures in images.

Homogeneity is measured for the images in Figs. 2–5 and are displayed in Tables 18–21.

From the summary presented in Tables 18–21, it is proved that the modified G-L FD operator provides a substantial improvement in terms of %H_{Imp} over the basic G-L FD operator. It is also noted that the homogeneity decreases with the

basic G-L FD operator when v is increased from 0 to a certain value around 0.5–0.6, after which, the homogeneity starts increasing. For the modified G-L FD operator, the range of values of v, for which homogeneity decreases gradually is 0–0.8. Therefore, the improvisation of the texture enhancing process is justified.

Considering these measures for the four images in Figs. 2–5, it is found that the maximum % of improvement that could be obtained by the basic G-L FD operator and the modified G-L FD operator in all the measures are approximated in Table 22.

Thus, it justified that the modified G-L FD operator is capable of providing outstanding performance when compared with the basic G-L FD operator. It is also found that the contrast measure is mostly improved by the proposed operator.

Table 18
Sample Image 1 - homogeneity.

Rotation offset Fractional order	0°				45°				90°				135°			
	G-L op.	%H _{Imp}	M G-L op.	%H _{Imp}	G-L op.	%H _{Imp}	M G-L op.	%H _{Imp}	G-L op.	%H _{Imp}	M G-L op.	%H _{Imp}	G-L op.	%H _{Imp}	M G-L op.	%H _{Imp}
Input Image	0.7635	0.00	0.7635	0.00	0.7197	0.00	0.7197	0.00	0.7258	0.00	0.7258	0.00	0.6771	0.00	0.6771	0.00
Output Image (v=0)	0.9045	18.47	0.9045	18.47	0.8913	23.85	0.8913	23.85	0.8983	23.76	0.8983	23.76	0.8691	28.36	0.8691	28.36
Output Image (v=0.05)	0.8875	16.24	0.8863	16.08	0.8745	21.51	0.8740	21.43	0.8842	21.81	0.8839	21.77	0.8486	25.33	0.8479	25.22
Output Image (v=0.15)	0.8509	11.45	0.8441	10.56	0.8300	15.33	0.8242	14.52	0.8418	15.97	0.8407	15.82	0.7950	17.42	0.7906	16.76
Output Image (v=0.25)	0.8063	5.61	0.7911	3.62	0.7785	8.17	0.7696	6.93	0.7946	9.47	0.7934	9.30	0.7372	8.87	0.7294	7.72
Output Image (v=0.35)	0.7645	0.13	0.7393	-3.17	0.7292	1.32	0.7140	-0.79	0.7473	2.96	0.7470	2.91	0.6809	0.57	0.6689	-1.21
Output Image (v=0.45)	0.7358	-3.63	0.6982	-8.55	0.6937	-3.61	0.6722	-6.60	0.7146	-1.55	0.7133	-1.73	0.6453	-4.69	0.6260	-7.54
Output Image (v=0.55)	0.7270	-4.77	0.6762	-11.43	0.6791	-5.65	0.6512	-9.52	0.7014	-3.36	0.7016	-3.34	0.6328	-6.54	0.6063	-10.45
Output Image (v=0.65)	0.7286	-4.57	0.6645	-12.96	0.6806	-5.43	0.6438	-10.55	0.6996	-3.62	0.6962	-4.08	0.6347	-6.26	0.6028	-10.98
Output Image (v=0.75)	0.7398	-3.10	0.6636	-13.08	0.6941	-3.56	0.6457	-10.28	0.7080	-2.46	0.7025	-3.22	0.6455	-4.67	0.6086	-10.12
Output Image (v=0.85)	0.7499	-1.78	0.6639	-13.04	0.7000	-2.73	0.6502	-9.66	0.7194	-0.88	0.7145	-1.56	0.6595	-2.60	0.6124	-9.56
Output Image (v=0.95)	0.7587	-0.63	0.6607	-13.46	0.7058	-1.93	0.6539	-9.15	0.7169	-1.23	0.7224	-0.47	0.6656	-1.69	0.6178	-8.76
Output Image (v=1)	0.7647	0.17	0.6606	-13.47	0.7154	-0.60	0.6560	-8.85	0.7215	-0.60	0.7266	0.10	0.6727	-0.65	0.6200	-8.44

Table 19
Sample Image 2 - homogeneity.

Rotation offset Fractional order	0°				45°				90°				135°			
	G-L op.	%H _{Imp}	M G-L op.	%H _{Imp}	G-L op.	%H _{Imp}	M G-L op.	%H _{Imp}	G-L op.	%H _{Imp}	M G-L op.	%H _{Imp}	G-L op.	%H _{Imp}	M G-L op.	%H _{Imp}
Input Image	0.5545	0.00	0.5545	0.00	0.5415	0.00	0.5415	0.00	0.5670	0.00	0.5670	0.00	0.5446	0.00	0.5446	0.00
Output Image (v=0)	0.5031	-9.27	0.5031	-9.27	0.4920	-9.14	0.4920	-9.14	0.5936	4.68	0.5936	4.68	0.4944	-9.22	0.4944	-9.22
Output Image (v=0.05)	0.4978	-10.22	0.4926	-11.18	0.4865	-10.17	0.4815	-11.08	0.5829	2.81	0.5812	2.50	0.4876	-10.47	0.4836	-11.20
Output Image (v=0.15)	0.4962	-10.52	0.4753	-14.29	0.4825	-10.90	0.4677	-13.63	0.5711	0.72	0.5703	0.58	0.4874	-10.50	0.4703	-13.64
Output Image (v=0.25)	0.4950	-10.73	0.4675	-15.70	0.4858	-10.28	0.4624	-14.62	0.5681	0.18	0.5624	-0.81	0.4855	-10.84	0.4622	-15.13
Output Image (v=0.35)	0.5066	-8.65	0.4622	-16.65	0.4909	-9.34	0.4576	-15.50	0.5675	0.09	0.5575	-1.68	0.4930	-9.47	0.4585	-15.81
Output Image (v=0.45)	0.5142	-7.28	0.4594	-17.15	0.4989	-7.87	0.4571	-15.58	0.5685	0.26	0.5583	-1.54	0.5032	-7.59	0.4573	-16.02
Output Image (v=0.55)	0.5244	-5.44	0.4573	-17.53	0.5093	-5.96	0.4590	-15.25	0.5737	1.17	0.5613	-1.02	0.5113	-6.10	0.4579	-15.91
Output Image (v=0.65)	0.5355	-3.44	0.4569	-17.60	0.5215	-3.69	0.4587	-15.29	0.5747	1.36	0.5634	-0.65	0.5235	-3.87	0.4594	-15.63
Output Image (v=0.75)	0.5427	-2.13	0.4561	-17.75	0.5294	-2.23	0.4610	-14.88	0.5745	1.32	0.5683	0.22	0.5288	-2.89	0.4599	-15.55
Output Image (v=0.85)	0.5493	-0.95	0.4561	-17.75	0.5368	-0.87	0.4639	-14.34	0.5734	1.13	0.5768	1.72	0.5353	-1.70	0.4631	-14.96
Output Image (v=0.95)	0.5563	0.31	0.4547	-18.01	0.5398	-0.31	0.4656	-14.01	0.5705	0.61	0.5828	2.78	0.5408	-0.69	0.4633	-14.93
Output Image (v=1)	0.5571	0.47	0.4557	-17.82	0.5396	-0.36	0.4676	-13.65	0.5649	-0.38	0.5853	3.22	0.5422	-0.43	0.4653	-14.56

Table 20
Sample Image 3 - homogeneity.

Rotation offset Fractional order	0°				45°				90°				135°			
	G-L op.	%H _{Imp}	M G-L op.	%H _{Imp}	G-L op.	%H _{Imp}	M G-L op.	%H _{Imp}	G-L op.	%H _{Imp}	M G-L op.	%H _{Imp}	G-L op.	%H _{Imp}	M G-L op.	%H _{Imp}
Input Image	0.7996	0.00	0.7996	0.00	0.7586	0.00	0.7586	0.00	0.7884	0.00	0.7884	0.00	0.7815	0.00	0.7815	0.00
Output Image (v=0)	0.8350	4.42	0.8350	4.42	0.8027	5.81	0.8027	5.81	0.8487	7.65	0.8487	7.65	0.8180	4.67	0.8180	4.67
Output Image (v=0.05)	0.8238	3.02	0.8209	2.66	0.7893	4.04	0.7869	3.73	0.8371	6.18	0.8360	6.04	0.8061	3.15	0.8037	2.84
Output Image (v=0.15)	0.8057	0.76	0.7966	-0.37	0.7672	1.13	0.7602	0.21	0.8172	3.65	0.8147	3.33	0.7861	0.59	0.7788	-0.35
Output Image (v=0.25)	0.7911	-1.06	0.7745	-3.15	0.7500	-1.14	0.7377	-2.76	0.8016	1.67	0.7970	1.09	0.7709	-1.36	0.7580	-3.01
Output Image (v=0.35)	0.7821	-2.19	0.7576	-5.26	0.7383	-2.68	0.7206	-5.01	0.7889	0.07	0.7832	-0.66	0.7613	-2.59	0.7420	-5.06
Output Image (v=0.45)	0.7785	-2.65	0.7450	-6.83	0.7319	-3.52	0.7088	-6.57	0.7826	-0.73	0.7746	-1.74	0.7564	-3.22	0.7312	-6.45
Output Image (v=0.55)	0.7758	-2.99	0.7353	-8.05	0.7297	-3.81	0.7009	-7.61	0.7772	-1.42	0.7688	-2.48	0.7548	-3.42	0.7239	-7.37
Output Image (v=0.65)	0.7794	-2.53	0.7299	-8.73	0.7325	-3.44	0.6974	-8.07	0.7771	-1.43	0.7668	-2.74	0.7575	-3.08	0.7204	-7.82
Output Image (v=0.75)	0.7849	-1.84	0.7282	-8.93	0.7382	-2.70	0.6986	-7.92	0.7799	-1.08	0.7701	-2.32	0.7627	-2.41	0.7209	-7.76
Output Image (v=0.85)	0.7896	-1.25	0.7261	-9.20	0.7442	-1.91	0.6999	-7.74	0.7812	-0.92	0.7724	-2.03	0.7682	-1.71	0.7210	-7.74
Output Image (v=0.95)	0.7969	-0.34	0.7250	-9.33	0.7537	-0.65	0.7030	-7.33	0.7858	-0.33	0.7775	-1.38	0.7772	-0.56	0.7237	-7.39
Output Image (v=1)	0.7996	-0.01	0.7265	-9.15	0.7571	-0.20	0.7066	-6.86	0.7869	-0.19	0.7809	-0.94	0.7800	-0.20	0.7265	-7.05

Table 21
Sample Image 4 - homogeneity.

Rotation offset Fractional order	0°				45°				90°				135°			
	G-L op.	%H _{Imp}	M G-L op.	%H _{Imp}	G-L op.	%H _{Imp}	M G-L op.	%H _{Imp}	G-L op.	%H _{Imp}	M G-L op.	%H _{Imp}	G-L op.	%H _{Imp}	M G-L op.	%H _{Imp}
Input Image	0.7895	0.00	0.7895	0.00	0.7535	0.00	0.7535	0.00	0.7956	0.00	0.7956	0.00	0.7573	0.00	0.7573	0.00
Output Image (v=0)	0.9080	15.01	0.9080	15.01	0.8933	18.56	0.8933	18.56	0.9198	15.61	0.9198	15.61	0.8950	18.19	0.8950	18.19
Output Image (v=0.05)	0.8931	13.12	0.8910	12.86	0.8764	16.32	0.8747	16.10	0.9069	14.00	0.9063	13.91	0.8785	16.00	0.8766	15.75
Output Image (v=0.15)	0.8605	8.99	0.8523	7.96	0.8393	11.39	0.8326	10.50	0.8783	10.40	0.8758	10.08	0.8419	11.18	0.8355	10.32
Output Image (v=0.25)	0.8215	4.05	0.8054	2.01	0.7944	5.43	0.7819	3.77	0.8440	6.09	0.8405	5.65	0.7980	5.37	0.7858	3.76
Output Image (v=0.35)	0.7757	-1.75	0.7481	-5.24	0.7429	-1.40	0.7224	-4.13	0.8039	1.05	0.7993	0.46	0.7462	-1.46	0.7261	-4.12
Output Image (v=0.45)	0.7456	-5.56	0.7035	-10.89	0.7088	-5.93	0.6773	-10.11	0.7737	-2.75	0.7683	-3.42	0.7126	-5.90	0.6820	-9.94
Output Image (v=0.55)	0.7579	-4.00	0.7016	-11.14	0.7204	-4.39	0.6772	-10.12	0.7796	-2.00	0.7663	-3.68	0.7244	-4.34	0.6811	-10.07
Output Image (v=0.65)	0.7589	-3.88	0.6943	-12.05	0.7208	-4.33	0.6730	-10.68	0.7788	-2.11	0.7685	-3.41	0.7248	-4.29	0.6776	-10.53
Output Image (v=0.75)	0.7778	-1.48	0.6993	-11.42	0.7409	-1.66	0.6806	-9.67	0.7915	-0.52	0.7756	-2.52	0.7445	-1.70	0.6851	-9.53
Output Image (v=0.85)	0.7855	-0.51	0.7009	-11.23	0.7479	-0.74	0.6851	-9.08	0.7967	0.15	0.7827	-1.62	0.7519	-0.71	0.6894	-8.97
Output Image (v=0.95)	0.7832	-0.79	0.6898	-12.63	0.7448	-1.15	0.6780	-10.02	0.7906	-0.62	0.7831	-1.57	0.7489	-1.11	0.6824	-9.89
Output Image (v=1)	0.7891	-0.05	0.6889	-12.74	0.7515	-0.27	0.6787	-9.93	0.7936	-0.25	0.7849	-1.34	0.7551	-0.29	0.6836	-9.73

Table 22
% of improvement - an analysis.

	G-L FD op.	M G-L FD op.
$%C_{imp}$	Around 50%	More than 100%
$%CoT_{imp}$	Around (5–6)%	Around –30%
$%E_{imp}$	Around –30%	Around –50%
$%H_{imp}$	Around –10%	Around –20%

5.5. Applications

5.5.1. Application in remote sensing image enhancement

Remote sensing methods are commonly used for applications such as defending environment protection, military surveillance and land mapping. But, there are issues like sensor limitation and atmospheric dispersion that may produce images with inadequate quality such as low contrast and blurring, which will be an obstacle for successful analysis. Therefore, improving the quality of remote sensing images is found to be significant.

Our proposed FD operator works well for enhancing remote sensing images. Two aerial images are considered for demonstration. Our proposed solution is compared with histogram equalization [8,9], basic G-L FD operator [12] and adaptive FD operator [30] to justify the potential of our approach over these approaches and the results are presented in Figs. 6 and 7. The results of adaptive FD operator presented in Figs. 6(d) and 7(d) are taken from [30].

As shown in Fig. 6 and 7, while the overall brightness of the images are well increased by histogram equalization [8,9], the texture details are least considered. Even though the basic G-L FD operator [12] and the adaptive G-L FD operator [30] provide higher efficiency in texture enhancement and better convergence rate, these methods have deficiency in considering the complexity and diversity of minute texture details. Therefore, these methods are able to provide only minimal enhancement for minute texture details. Comparing with the adaptive approach [30], the proposed G-L FD operator considers to include autocorrelation feature in the filter itself and thus, this method is able to enhance the minute

texture details throughout the image. Thus, the proposed FD operator is able to achieve around 20–30% more enhancement than the previous approaches.

In order to show the capability of our approach in enhancing specific regions of remote sensing images, the results of the proposed filter are compared with those of basic G-L FD operator [12] and adaptive G-L FD operator [30] in Figs. 8 and 9.

Since, the autocorrelation is not considered in the basic G-L FD operator [12] and some pixel values are overestimated, (see Fig. 8 (b)), particular regions of the image such as the building roofs seem extremely bright. Due to the adaptive nature of G-L FD operator [30], the visibility of specific regions like rivers and highways shown in Fig. 8(c) are enhanced, however, other details are less concentrated. It is noted from Fig. 8(d) that the degree of enhancement becomes higher with our proposed FD operator. It is also observed that our proposed FD operator improves visibility evenly in all parts of the image by enhancing of minute texture details everywhere by imposing autocorrelation feature. In addition, the texture details around the river and highway portions are more noticeable than the other methods. Therefore, it is justified that texture is enhanced in all parts of images by concentrating on minute texture details throughout the image. This is not the case with adaptive FD operators that concentrate on particular regions based on the value chosen for FD order.

In the second aerial image shown in Fig. 9, the minute texture details are fine discriminated even in smooth areas such as sea waves by enhancement through our proposed solution.

5.5.2. Application in medical image enhancement

Medical images are usually characterized as low contrast images. The process of acquiring high contrast images with the imaging device is little slow. Particularly, in case of X-ray image acquisition, the process needs higher X-ray dose to be given to patients and thereby is not desirable. Thus, enhancing medical images turns into a significant post-processing in the related applications. Our proposed FD operator provides satisfactory results for medical image enhancement. The enhancement result

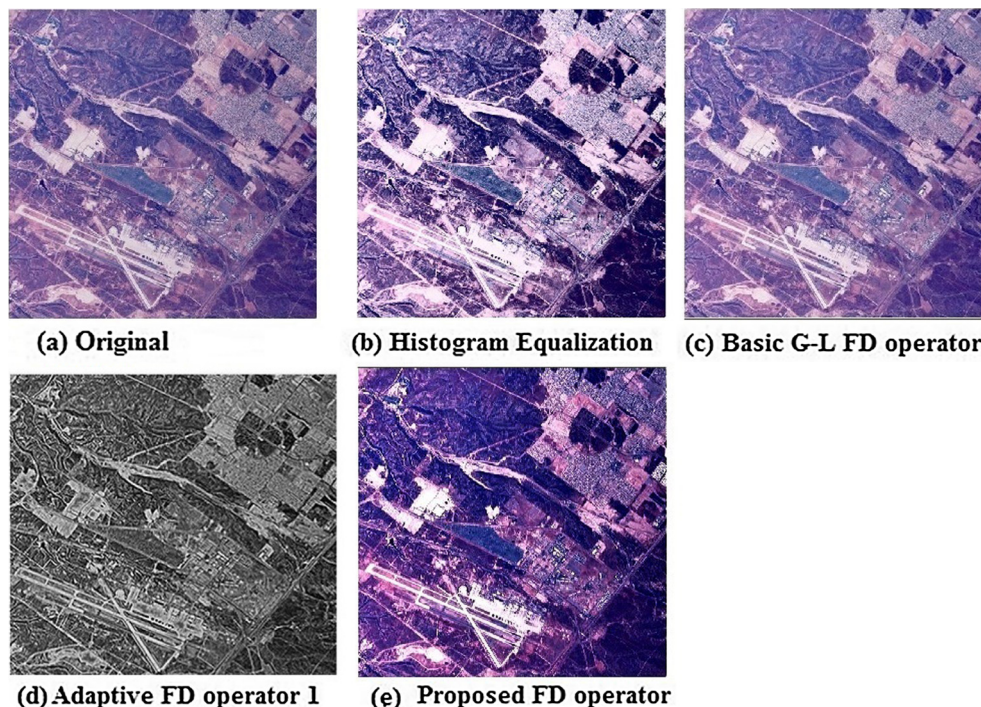


Fig. 6. Aerial Image 1 - texture enhancement - comparison.

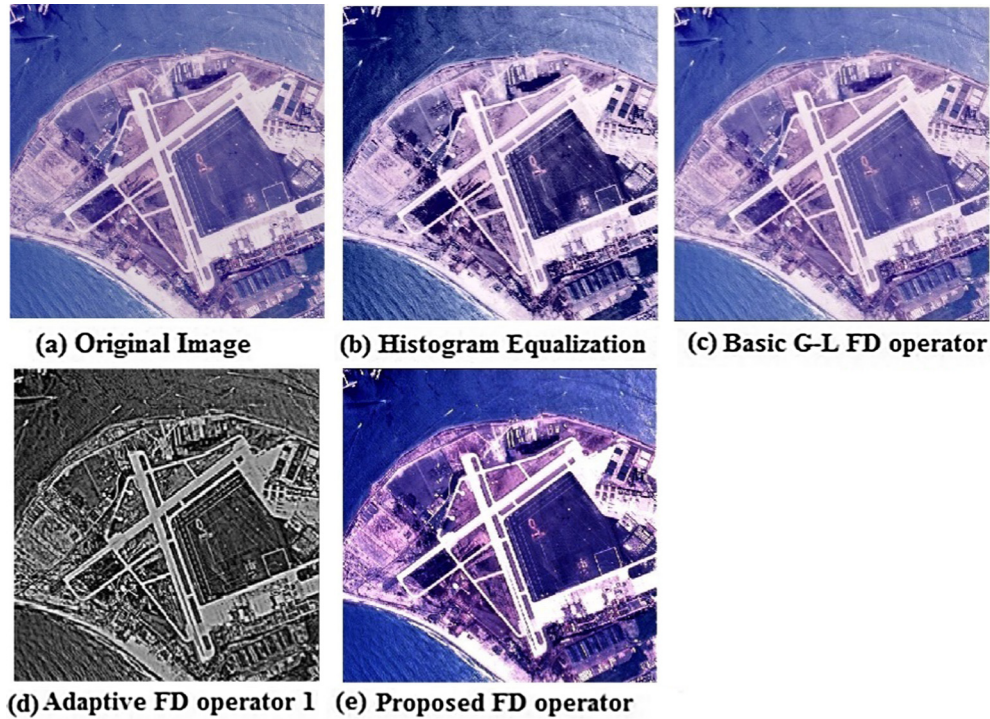


Fig. 7. Aerial Image 2 - texture enhancement - comparison.

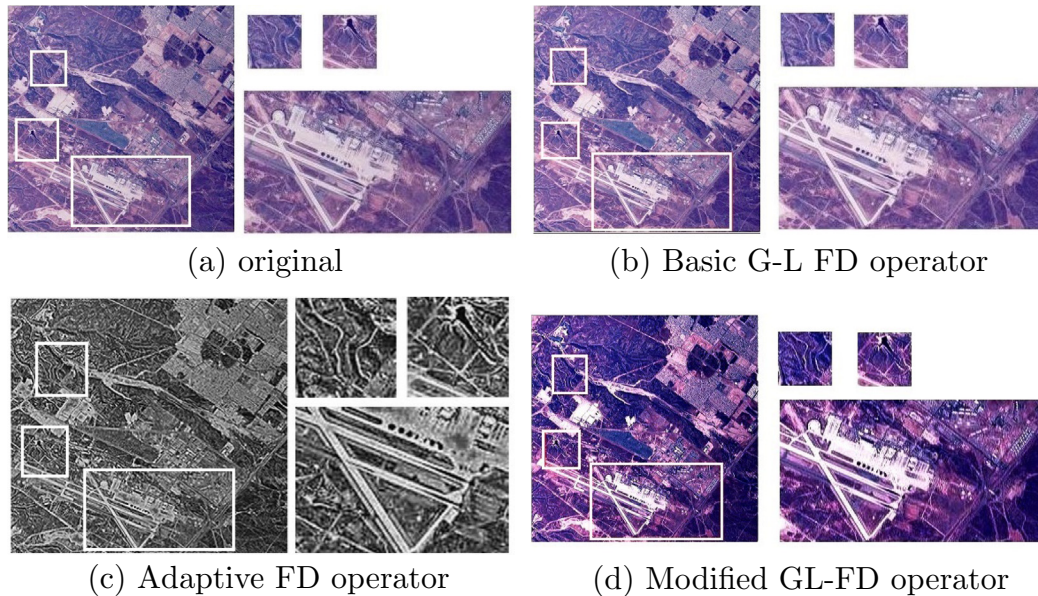


Fig. 8. Enhancement results of aerial Image 1: three local regions highlighted in white are enlarged and placed at the right of each image.

for chest X-ray image is compared with basic G-L FD operator [12], adaptive FD operators [30,31] and the results are displayed in Fig. 10. The results of adaptive FD operator presented in Fig. 10 (c) and (d) are taken from [30,31].

The basic G-L FD operator is able to provide only minimal enhancement for textural information, whereas, the two adaptive operators attempt to enhance the texture details by fixing the fractional differential order in an adaptive manner. Comparing with these adaptive approaches, the proposed G-L FD operator enhances the minute texture details in the image by incorporating autocorrelation feature in the filter itself. Thus, our proposed FD operator

provides up to 20–30% more enhancement for the chest X-ray image than the basic G-L FD operator and the two adaptive FD operators.

The potential of the proposed G-L FD operator for enhancing the chest X-ray image is proved by comparing the results of basic G-L FD operator [12], two adaptive G-L FD operator [30] and the proposed operator in Fig. 11. The basic G-L FD operator [12] provides marginal enhancement in terms of textural information, however lacks in enhancing specific regions like shoulder joint and rib cage. With adaptive FD operators, the rib cage details are over-enhanced as can be seen from Fig. 11(b). Although, the adaptive operators

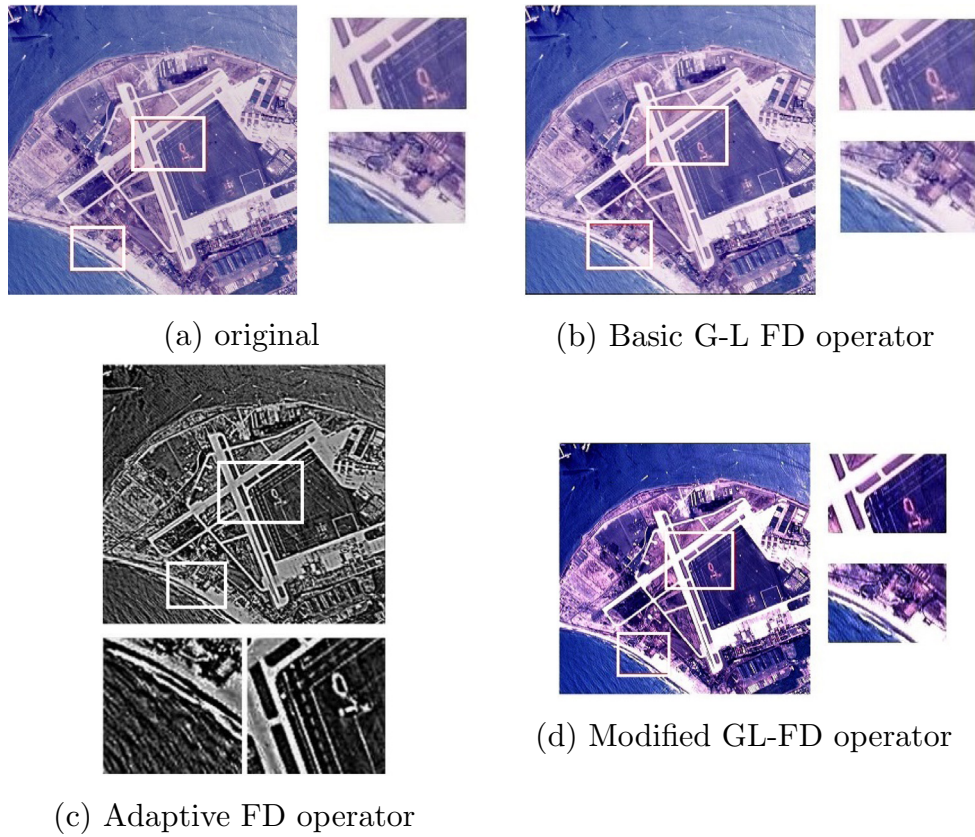


Fig. 9. Enhancement results of aerial Image 2: two local regions highlighted in white are enlarged and placed at the right of each image.

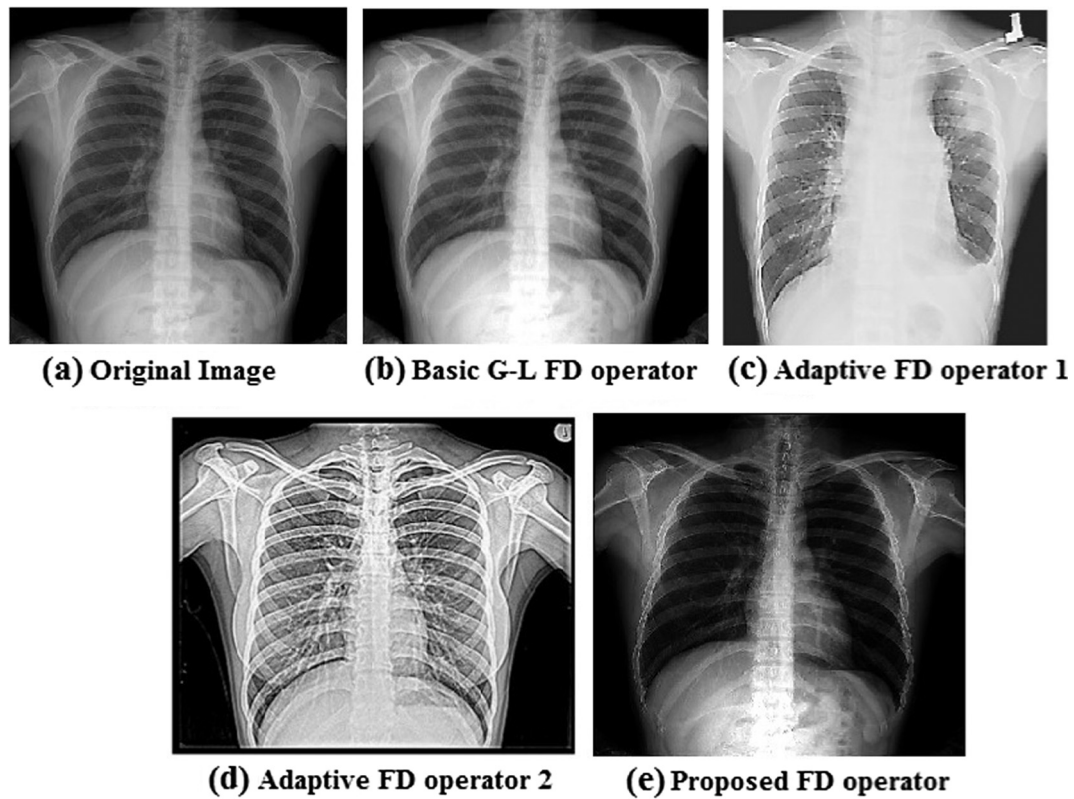


Fig. 10. The X-ray image of human chest - comparison of different FD operators.

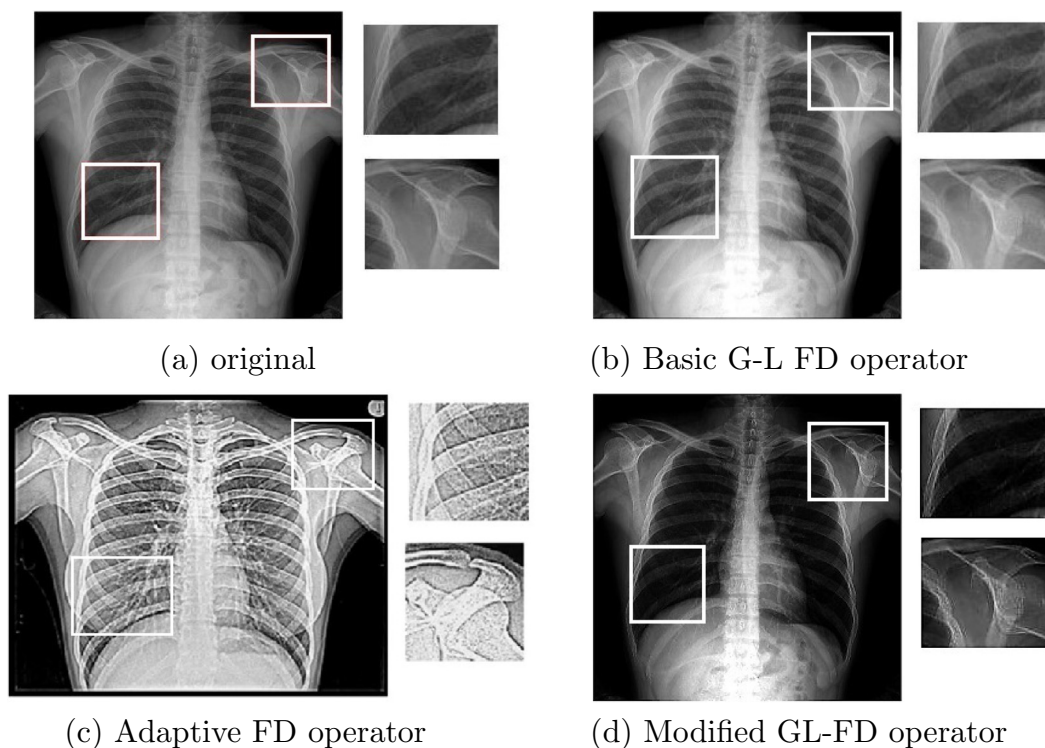


Fig. 11. Enhancement results of the chest X-ray image: two local regions highlighted in white are enlarged and placed at the right of each image.

efficiently enhance the shoulder joint and ribcage details, the modified G-L FD operator produces better enhancement for these specific regions. As well, this modified operator enhances the overall image by improving minute texture details due to the inclusion of autocorrelation feature.

6. Conclusion

For texture enhancement in gray scale and colour images, the G-L fractional differential operator is modified using the fact that large amount of autocorrelation exists between pixels in local neighborhoods. The filter coefficients that are zero in the basic G-L FD filter are made non-zero by distributing the autocorrelation feature across pixels in a neighborhood. The modified FD operator is applied to textured images; texture enhancement is obtained and compared with histogram equalization, basic G-L FD operator and adaptive FD operator. The experiments by visual analysis proved that the proposed operator is able to provide better enhancement than the basic G-L FD filter.

As can be seen from the analysis shown in Table 22, it is concluded that the modified G-L FD operator outperforms the basic G-L FD operator. It is also noted that the rate at which these measures attain their improvement (either increasingly or decreasingly) by the increase in FD order is appreciably higher with the modified G-L FD operator than with the basic G-L FD operator. The optimum value fractional order ν is found to lie in the range 0.5–0.7.

Our proposed solution is demonstrated in enhancing the textural details carrying vital information in different types of images such as remote sensing images and medical images. In future, it is planned to use this operator for pre-processing step for image segmentation. In our proposed approach, the optimum value for the FD order is obtained by experiments. In future, the proposed method will be extended to make the fractional order adaptive one.

References

- [1] Haralick RM, Shanmugam K, Dinstein IH. Textural features for image classification. *IEEE Trans Syst Man Cybern* 1973(6):610–21.
- [2] Ojala T, Valkealahti K, Oja E, Pietikäinen M. Texture discrimination with multidimensional distributions of signed gray-level differences. *Pattern Recogn* 2001;34(3):727–39.
- [3] Chakraborty D, Thakur S, Jeyaram A, Murthy YK, Dadhwal V. Texture analysis for classification of Riset-II images. In: XXII ISPRS congress, Melbourne, Australia, vol. 25; 2012.
- [4] Danesh H, Kafieh R, Rabbani H, Hajizadeh F. Segmentation of choroidal boundary in enhanced depth imaging OCTs using a multiresolution texture based modeling in graph cuts. *Comput Math Methods Med* 2014.
- [5] Polesel A, Ramponi G, Mathews VJ, et al. Image enhancement via adaptive unsharp masking. *IEEE Trans Image Process* 2000;9(3):505–10.
- [6] Narasimhan SG, Nayar SK. Contrast restoration of weather degraded images. *IEEE Trans Pattern Anal Mach Intell* 2003;25(6):713–24.
- [7] Saleem A, Beghdadi A, Boashash B. Image fusion-based contrast enhancement. *EURASIP J Image Video Process* 2012;2012(1):1–17.
- [8] Magudeeswaran V, Ravichandran C. Fuzzy logic-based histogram equalization for image contrast enhancement. *Math Probl Eng* 2013.
- [9] Jung S-W. Image contrast enhancement using color and depth histograms. *IEEE Signal Process Lett* 2014(21):382–5.
- [10] Ortigueira MD. Riesz potential operators and inverses via fractional centred derivatives. *Int J Math Math Sci* 2006.
- [11] Neel MC, Joelson M. Generalizing Grünwald-Letnikov's formulas for fractional derivatives.
- [12] Pu Y-F, Zhou J-L, Yuan X. Fractional differential mask: a fractional differential-based approach for multiscale texture enhancement. *IEEE Trans Image Process* 2010;19(2):491–511.
- [13] Chen M-H, Lee D, Pavlidis T. Residual analysis for feature detection. *IEEE Trans Pattern Anal Mach Intell* 1991(1):30–40.
- [14] Xie X, Mirmehdi M. A galaxy of texture features. *Handbook Texture Anal* 2008:375–406.
- [15] Selvarajan S. An enhanced technique for image indexing and retrieval with orientation features using autocorrelation function. *Int J Innovative Technol Creative Eng* 2015(2):259–64.
- [16] Wang B, Zhang L. Supervised texture segmentation using wavelet transform. In: Neural networks and signal processing, 2003. Proceedings of the 2003 international conference on, vol. 2. IEEE; 2003. p. 1078–82.
- [17] Cossu R, Jermyn IH, Zerubia J. Texture discrimination using multimodal wavelet packet subbands. In: Image processing, 2004. ICIP'04. 2004 international conference on, vol. 3. IEEE; 2004. p. 1493–6.
- [18] Li C-T, Chiao R. Unsupervised texture segmentation using multiresolution hybrid genetic algorithm. In: Image processing, 2003. ICIP 2003. Proceedings. 2003 international conference on, vol. 2. IEEE; 2003. p. II-1033.

- [19] Zhao B, Zhu Z, Mao E, Song Z. Image segmentation based on ant colony optimization and k-means clustering. In: Automation and logistics. 2007 IEEE international conference on. IEEE; 2007. p. 459–63.
- [20] Gordont DK, Phtlipson Clears WR. A texture-enhancement procedure for separating orchard from forest in thematic mapper data. *Int J Remote Sens* 1986;7(2):301–4.
- [21] Ghose S, Oliver A, Marti R, Lladó X, Freixenet J, Vilanova JC, et al. Prostate segmentation with texture enhanced active appearance model. In: Signal-image technology and internet-based systems (SITIS). 2010 Sixth international conference on. IEEE; 2010. p. 18–22.
- [22] Liu Y. Remote sensing image enhancement based on fractional differential. In: Computational and information sciences (ICCIS). 2010 International conference on. IEEE; 2010. p. 881–4.
- [23] Zuo H, Wang Y, Yang X, Wang X. Fabric defect detection based on texture enhancement. In: Image and signal processing (CISP). 2012 5th international congress on. IEEE; 2012. p. 876–80.
- [24] Melbourne A, Cahill N, Tanner C, Modat M, Hawkes D, Ourselin S. Using fractional gradient information in non-rigid image registration: application to breast MRI. In: SPIE medical imaging, international society for optics and photonics; 2012. p. 83141Z–83141Z.
- [25] Ghita O, Ilea DE, Whelan PF. Texture enhanced histogram equalization using tv-image decomposition. *IEEE Trans Image Process* 2013;22(8):3133–44.
- [26] Mathieu B, Melchior P, Oustaloup A, Ceyral C. Fractional differentiation for edge detection. *Signal Process* 2003;83(11):2421–32.
- [27] Qing C. A fractional differential approach to low contrast image enhancement. *Int J Knowl Lang Process* 2012;3(2):20–9.
- [28] Jalab HA, Ibrahim RW. Texture enhancement for medical images based on fractional differential masks. *Discrete Dynamics Nat Soc* 2013.
- [29] Pu Y, Siarry P, Zhou J, Liu Y, Zhang N, Huang G, et al. Fractional partial differential equation denoising models for texture image. *Sci China Inform Sci* 2014;57(7):1–19.
- [30] Hu F, Si S, San Wong H, Fu B, Si M, Luo H. An adaptive approach for texture enhancement based on a fractional differential operator with non-integer step and order. *Neurocomputing* 2015;158:295–306.
- [31] Li B, Xie W. Adaptive fractional differential approach and its application to medical image enhancement. *Comput Electr Eng* 2015;45:324–35.
- [32] Yu Q, Vegh V, Liu F, Turner I. A variable order fractional differential-based texture enhancement algorithm with application in medical imaging. *PLoS One* 2015;10(7):e0132952.
- [33] Yang Z, Lang F, Yu X, Zhang Y. The construction of fractional differential gradient operator. *J Comput Inform Syst* 2011;7(12):4328–42.
- [34] Zhang Y, Pu Y, Zhou J. Construction of fractional differential masks based on Riemann-Liouville definition. *J Comput Inform Syst* 2010;6(10):3191–9.
- [35] Griffith DA. Spatial autocorrelation. A Primer. Washington DC: Association of American Geographers.
- [36] Brodatz P. Textures: a photographic album for artists and designers, vol. 66. Dover New York. <<http://www.ux.uis.no/tranden/brodatz.html>> [accessed 21 December 2015].
- [37] U. of Oulu. Outex – texture database. <<http://www.outex.oulu.fi/>> [accessed 18 January 2016].
- [38] U.U. of Southern California. Database of aerial images. <<http://sipi.usc.edu/database/database.php?volume=aerials>> [accessed 2 February 2016].
- [39] Database of Medical images. <<http://peipa.essex.ac.uk/benchmark/databases/>> [accessed 2 September 2016].



S. Hemalatha received her BE in Computer Science and Engineering from the University of Madras, TN, India in 2000. She completed her M.Tech in Computer Science and Engineering in 2004 and is currently pursuing Ph.D in the Image Processing domain. She is working as an Assistant Professor (Selection Grade) in VIT University, TN, India. She has about 15 years of teaching experience in the field of Computer Science and Engineering. Her research interests include Image Processing, Pattern Recognition, Image Classification and Segmentation. She published papers with International journals and international conferences in these areas.



S Margret Anuncia received her BE in Computer Science and Engineering from Bharathidasan University, TN, India in 1993. She completed her M.E in Software Engineering in 2001 and P.hD in the field of Knowledge Engineering in 2008. She is currently working as a Professor in VIT University, TN, India. She has about 20 years of teaching experience in the field of Computer Science and Engineering. Her research interests include Image Processing, Pattern Recognition, Knowledge Engineering and Software Engineering. She published many papers with International journals and international conferences in these areas.